Design of Frequency Selective Surface (FSS) for Mobile Signal Shielding

By

Mohammed T. Al Haddad

Supervisor

Dr. Talal F. Skaik

A Thesis Submitted to the Islamic University Of Gaza for the Degree of Master in communication Engineering

Department of Electrical Engineering

The Islamic University Of Gaza – IUG

Palestine

January 2016

Abstract

The purpose of this project is to design novel structures of frequency selective surfaces (FSS). FSSs have been the subject of intensive investigation for their widespread applications in communication and radar systems. For practical applications, it is desired to realize a FSS with miniaturized elements and a stable frequency response for different polarizations and incident angles. But these features are difficult to obtain through traditional designs.

The focus in this thesis was to shield the signals of mobile communications, and five FSS models have been designed to achieve that based on 2D periodic arrays. The simulations are done using CST Microwave Studio.

First design which is double square loop microstrip structure covered GSM900 and GSM1800 bands while the second design is a novel microstrip model that covered the bands GSM900, GSM1800 and LTE. The third design is similar to previous designs but with glass substrate to be suitable for wide buildings, and the fourth model covers more bands including GSM900, GSM1800, 3G (UMTS) and LTE. The last model is designed to be suitable to the outdoor applications and it is made from double wired net joined with iron cylinders and it covers the bands GSM900, GSM1800 and 3G.

The simulation results showed good performance for scattering parameters for different polarizations and also various incident angles.

Acknowledgement

First and foremost, I would like to express my gratitude and appreciation to my supervisor, Dr Talal F. Skaik, for his patient guidance, encouragement, precious advice and suggestions through the whole project. Also I like to thank Dr. Ammar Abu Hadrouss and Dr. Tamer Abu Foul for acceptance to examine my thesis. I would also like to extend my sincere thanks to all colleagues in communication group who gave me comprehensive knowledge during the past two academic years. Also I like to extend my sincere thanks to my father and mother to moral support and encouragement before and during the study period.

Finally, extend deep thanks and appreciation to my beloved family for their loving consideration and continuous support , especially for my dear wife for all the support and care during the study period.

Table of contents

CHAPTER 1: INTRODUCTION 9

1.1 BACKGROUND 9
1.2 APPLICATIONS 10
1.3 GENERATIONS OF MOBILE COMMUNICATION SYSTEMS 11
1.3.1 First generation 12
1.3.2 Second generation 12
1.3.3 Third generation (3G) 13
1.3.4 Fourth generation 16
1.4 GLOBAL MOBILE SUBSCRIBERS AND MARKET SHARE BY TECHNOLOGY 17
1.5 FREQUENCY BANDS OF GENERATIONS 17
1.5.1 Frequencies of GSM 900-1800 bands 17
1.5.2 Frequencies of 3G bands 18
1.5.3 Frequencies of 4G Bands 19
1.6 THESIS OBJECTIVE 22
1.7 THESIS OVERVIEW 22

CHAPTER 2: FREQUENCY SELECTIVE SURFACE THEORY 23

2.1 THE RELEVANT CONCEPTS IN ELECTROMAGNETIC THEORY 23
2.2 FILTER GEOMETRIES AND EQUIVALENT CIRCUITS 24
2.3 STRIP GRATING FILTERS 25
2.4 MESH FILTERS 27
2.5 CROSS-MESH FILTERS 28
2.6 ANALYSIS OF MORE COMPLEX STRUCTURES 29
2.6.1 Square Loop FSS 29
2.6.2 Jerusalem Cross 32
2.7 A BRIEF OF MOST COMMON FSS GEOMETRIES 35
2.8 LITERATURE REVIEW 36

CHAPTER 3: DESIGNS AND SIMULATIONS OF FREQUENCY SELECTIVE SURFACES 38

3.1 INTRODUCTION 38
3.2 DESIGNS AND SIMULATIONS: 38
3.2.1 Goals of designs 38
3.2.2 Simulation Software CST 38
3.3 BASICS OF THE DESIGNS 38
3.4 BANDSTOP DOUBLE SQUARE LOOP FSS 39

3.4.1 Structure of FSS *39*
3.4.2 Simulation results *40*
3.5 TRI BANDSTOP OPEN LOOP FSS WITH FR SUBSTRATE 42
3.5.1 Structure of FSS *42*
3.5.2 Simulation results *43*
3.6 TRI BANDSTOP OPEN LOOP FSS WITH GLASS (PYREX) SUBSTRATE 47
3.6.1 Structure of FSS *48*
3.6.2 Simulation results *49*
3.7 QUAD BANDSTOP E_SHAPE FSS 52
3.7.1 Structure of FSS *52*
3.7.2 Simulation results *54*
3.7.3 The effect of changing the widths of elements *55*
3.8 DUAL BANDSTOP DOUBLE WIRED SQUARE LOOP FSS 56
3.8.1 Structure of FSS *57*
3.8.2 Simulation results *58*
CHAPTER 4: CONCLUSION 61
4.1 SUMMARY 61
4.1.1 First design (Bandstop double square loop FSS) *61*
4.1.2 Second design (Tri bandstop open loop FSS with FR substrate) *61*
4.1.3 Third design (Tri bandstop open loop FSS with glass (pyrex) substrate) *62*
4.1.4 Fourth design (Quad bandstop E_shape FSS) *62*
4.1.5 Fifth design (Dual Bandstop double wired square loop FSS) *63*
4.2 FUTURE WORK 63
REFERENCES 64

List of Figures

FIGURE 1.1: STRUCTURES OF FSS 10
FIGURE 1.2: MARSCHALS QUASI-OPTICAL FEED TRAIN 11
FIGURE 1.3: TIME DIVISION MULTIPLE ACCESS 13
FIGURE 1.4: CODE DIVISION MULTIPLE ACCESS 13
FIGURE 1.5: GLOBAL MOBILE SUBSCRIBERS AND MARKET SHARE BY TECHNOLOGY 17
FIGURE 1.6: GSM (GROUP SPECIAL MOBILE) - GLOBAL SYSTEM FOR MOBILE COMMUNICATIONS - MOST POPULAR STANDARD FOR PHONES IN THE WORLD. GSM 900 / GSM 1800 MHZ ARE USED IN MOST PARTS OF THE

WORLD: EUROPE, ASIA, AUSTRALIA, MIDDLE EAST, AND AFRICA. GSM 850 / GSM 1900 MHZ ARE USED IN THE UNITED STATES, CANADA, MEXICO AND MOST COUNTRIES OF S. AMERICA....18
FIGURE 1.7 : FREQUENCIES SEPARATED BY GAP....19
FIGURE 2.1: (A) PATCH ELEMENTS, (B) APERTURE ELEMENTS....23
FIGURE 2.2: (A) ELECTRON IN FILTER PLANE UNDERGOES OSCILLATIONS DRIVEN BY SOURCE WAVE, (B) ELECTRON CONSTRAINED TO MOVE ALONG WIRE CANNOT UNDERGO OSCILLATIONS....24
FIGURE 2.3: IF THE E-FIELD IS PERPENDICULAR TO THE STRIPS THE FILTER SWITCHES BETWEEN STATES A AND B, IF IT IS PARALLEL TO THE STRIP THE FILTER SWITCHES BETWEEN C AND D....25
FIGURE 2.4: STRIP-GRATING FILTERS AND ITS EQUIVALENT CIRCUIT....25
FIGURE 2.5: PLANE WAVE INCIDENT ON AN INDUCTIVE STRIP GRATING, FOR A CAPACITIVE STRIP GRATING EXCHANGE THE INCIDENT ELECTRIC FIELD E FOR A MAGNETIC FIELD H....26
FIGURE 2.6: MESH FILTERS AND ITS EQUIVALENT CIRCUIT....28
FIGURE 2.7: CROSS-MESH FILTERS....29
FIGURE 2.8: A) LAYOUT OF SQUARE LOOP ARRAYS, B) EQUIVALENT CIRCUIT....30
FIGURE 2.9: ANALYSIS OF SQUARE LOOP FSS....30
FIGURE 2.10: EQUIVALENT CIRCUIT FOR SQUARE LOOP....31
FIGURE 2.11: JERUSALEM CROSS PERIODIC ARRAY....33
FIGURE 2.12: EQUIVALENT CIRCUIT OF JERUSALEM CROSS....33
FIGURE 2.13: FREQUENCY RESPONSE OF JERUSALEM CROSS....33
FIGURE 2.14: JERUSALEM CROSS ETCHED IN DIELECTRIC SLAB....34
FIGURE 3.1: A) DIMENSIONS OF SQUARE LOOP FSS, B) SIDE VIEW OF THE MODEL....39
FIGURE 3.2: A) PERIODIC FSS, B) FSS MODEL WITH INCIDENT PLANE WAVE....40
FIGURE 3.3: SIMULATION RESULTS OF DUAL-BANDSTOP FSS FOR TM POLARIZATION....41
FIGURE 3.4: SIMULATION RESULTS OF DUAL-BANDSTOP FSS FOR TE POLARIZATION....41
FIGURE 3.5: OVERALL VIEW OF THE UNIT CELL MODEL....42
FIGURE 3.6: A) DIMENSIONS OF TOP VIEW MODEL, B) SIDE VIEW OF THE MODEL....43
FIGURE 3.7: PERIODIC CELLS....44
FIGURE 3.8: SIMULATION RESULTS OF TRI-BANDSTOP FSS FOR TE POLARIZATION....44
FIGURE 3.9: SIMULATION RESULTS OF TRI-BANDSTOP FSS FOR TM POLARIZATION....45
FIGURE 3.10: TRANSMISSION BANDWIDTHS AT 900/1800 MHZ AND LTE BAND FOR TE POLARIZATION AT THETA=0....46
FIGURE 3.11: TRANSMISSION BANDWIDTHS AT 900/1800 MHZ AND LTE BAND FOR TE POLARIZATION AT THETA=30....46
FIGURE 3.12: TRANSMISSION BANDWIDTHS AT 900/1800 MHZ AND LTE BAND FOR TM POLARIZATION AT THETA=0....47
FIGURE 3.13: TRANSMISSION BANDWIDTHS AT 900/1800 MHZ AND LTE BAND FOR TM POLARIZATION AT THETA=30....47
FIGURE 3.14: OVERALL VIEW OF THE UNIT CELL MODEL....48
FIGURE 3.15: A) DIMENSIONS OF TOP VIEW MODEL, B) SIDE VIEW OF THE MODEL....48
FIGURE 3.16: SIMULATION RESULTS OF TRI-BANDSTOP FSS FOR TE POLARIZATION....49

FIGURE 3.17: SIMULATION RESULTS OF TRI-BANDSTOP FSS FOR TM POLARIZATION 50
FIGURE 3.18: TRANSMISSION BANDWIDTHS AT 900/1800 MHZ AND LTE BAND FOR TE POLARIZATION AT THETA=0 51
FIGURE 3.19: TRANSMISSION BANDWIDTHS AT 900/1800 MHZ AND LTE BAND FOR TE POLARIZATION AT THETA=30 51
FIGURE 3.20: TRANSMISSION BANDWIDTHS AT 900/1800 MHZ AND LTE BAND FOR TM POLARIZATION AT THETA=0 52
FIGURE 3.21: TRANSMISSION BANDWIDTHS AT 900/1800 MHZ AND LTE BAND FOR TM POLARIZATION AT THETA=30 52
FIGURE 3.22: OVERALL VIEW OF THE UNIT CELL MODEL 53
FIGURE 3.23: A) DIMENSIONS OF TOP VIEW MODEL, B) SIDE VIEW OF THE MODEL 53
FIGURE 3.24: PERIODIC CELLS 54
FIGURE 3.25: SIMULATION RESULTS OF QUAD-BANDSTOP FSS FOR TE POLARIZATION 55
FIGURE 3.26: SIMULATION RESULTS OF QUAD-BANDSTOP FSS FOR TE POLARIZATION WITH VARYING THE ELEMENTS WIDTH 55
FIGURE 3.27: COMPARISON BETWEEN TE AND TM POLARIZATION 56
FIGURE 3.28: DIMENSIONS OF TOP VIEW MODEL 57
FIGURE 3.29: PERIODIC SQUARE CELLS 58
FIGURE 3.30: SIMULATION RESULTS OF TRI-BANDSTOP FSS FOR TE POLARIZATION 59
FIGURE 3.31: SIMULATION RESULTS OF TRI-BANDSTOP FSS FOR TM POLARIZATION 59
FIGURE 3.32: TE AND TM POLARIZATION AT THETA=0 60
FIGURE 3.33: TE AND TM POLARIZATION AT THETA=40 60

List of Tables

TABLE 1.1: 2G / 3G CELLULAR WIRELESS DATA TRANSPORT TERMINOLOGY 15
TABLE 1.2: (A) WIMAX RELEASE 2.0 (802.16M) TECHNICAL SPECIFICATIONS, (B) LTE-ADVANCED TECHNICAL SPECIFICATIONS 16
TABLE 1.3: 3G UMTS FREQUENCY BANDS – FDD 18
TABLE 1.4: FDD LTE BANDS AND FREQUENCIES 20
TABLE 1.5: TDD LTE BANDS AND FREQUENCIES 21
TABLE 2.1: A BRIEF OF MOST COMMON FSS GEOMETRIES AND ITS EQUIVALENT CIRCUITS 35
TABLE 3.1: DIMENSIONS OF THE DESIGN 39
TABLE 3.2: -10 DB TRANSMISSION BANDWIDTHS AT 900/1800 MHZ FOR TM POLARIZATION 41
TABLE 3.3: -10 DB TRANSMISSION BANDWIDTHS AT 900/1800 MHZ FOR TE POLARIZATION 42
TABLE 3.4: DIMENSIONS OF THE DESIGN 43
TABLE 3.5: -10 DB TRANSMISSION BANDWIDTHS AT 900/1800 MHZ AND LTE BAND FOR TE POLARIZATION 45
TABLE 3.6: : -10 DB TRANSMISSION BANDWIDTHS AT 900/1800 MHZ AND LTE BAND FOR TM POLARIZATION 46

TABLE 3.7: DIMENSIONS OF THE DESIGN 49
TABLE 3.8: -10 DB TRANSMISSION BANDWIDTHS AT 900/1800 MHZ AND LTE BAND FOR TE POLARIZATION 50
TABLE 3.9 : -10 DB TRANSMISSION BANDWIDTHS AT 900/1800 MHZ AND LTE BAND FOR TM POLARIZATION.....51
TABLE 3.10: DIMENSIONS OF THE DESIGN 54
TABLE 3.11: DIMENSIONS OF THE DESIGN 57
TABLE 3.12: -10 DB TRANSMISSION BANDWIDTHS AT 900/1800 MHZ AND 3G BAND FOR TE POLARIZATION.....60
TABLE 3.13: -10 DB TRANSMISSION BANDWIDTHS AT 900/1800 MHZ AND LTE BAND FOR TM POLARIZATION.....60
TABLE 4.1: S_{21} (DB) AT DESIRED FREQUENCIES AT THETA = 0^0 61
TABLE 4.2: TABLE 1:s_{21} (DB) AT DESIRED FREQUENCIES AT THETA = 45^0.....61
TABLE 4.3: s_{21} (DB) AT DESIRED FREQUENCIES AT THETA = 0^0.....61
TABLE 4.4: s_{21} (DB) AT DESIRED FREQUENCIES AT THETA = 30^0 62
TABLE 4.5: s_{21} (DB) AT DESIRED FREQUENCIES AT THETA = 0^0.....62
TABLE 4.6: s_{21} (DB) AT DESIRED FREQUENCIES AT THETA = 30^0 62
TABLE 4.7:s_{21} (DB) AT DESIRED FREQUENCIES AT THETA = 0^0 62
TABLE 4.8: s_{21} (DB) AT DESIRED FREQUENCIES AT THETA = 0^0.....63
TABLE 4.9: s_{21} (DB) AT DESIRED FREQUENCIES AT THETA = 30^0 63

Chapter 1: Introduction

1.1 Background:

Today the world is witnessing a significant increase in the use of mobile devices, which leads companies to expand mobile networks to include all walks of life including the installation of macro cells to amplify the signals within the buildings themselves.

Some facilities contain sensitive electronic devices could be affected by these signals, such as labs, In addition, some of the bodies and institutions want to isolate some places communication devices for security considerations, such as prisons.

Moreover, some places prevent the use of mobile devices, such as intensive care rooms in hospitals, and places of worship. Jammers are used to achieve that, but they need a source of energy that can cause undesirable effects on some ultra-sensitive devices.

Other technology used to achieve the desired shielding is frequency selective surface (FSS).

A frequency selective surface is a spatial electromagnetic filter includes at least one frequency selective layer made up of an array of electrically conductive elements (patch elements) or aperture elements etched on a dielectric substrate.

The selective surface works as band pass or band stop filter. The patch element array behaves as a band stop filter and the aperture element array acts as a band pass filter.

The frequencies transmitted or reflected depend on the resonance of the shapes of conductive elements. The most common shapes used in FSS are simple straight dipole, circular loop, cross dipole, three-legged dipole, square loop and Jerusalem Cross. The four major groups of FSS elements are shown in Figure.1.1. Elements are ordered from most narrow-banded on the left to most wide-banded on the right [1]

There are two types of FSS one is passive which is used in fixed systems, and the other is active which can be tunable and gives more flexibility, this type is used mainly for tunable radome or adaptive screening of un-wanted wireless transmissions.[2]

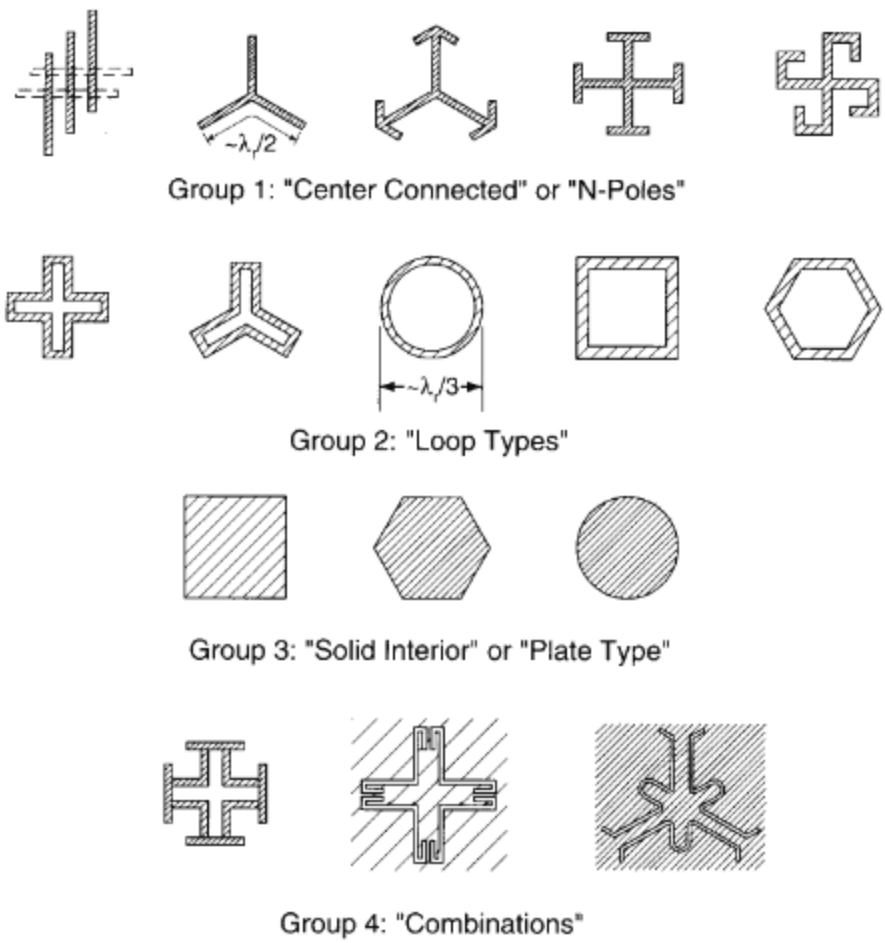

Figure 1.1: structures of FSS

1.2 Applications:

Frequency selective surfaces are used in a wide variety of applications such as below:

- The realization of reflector antenna systems which enables two or more feeds to share the same parabolic main reflector simultaneously.
- Radome design, FSS used with a protective radome to reduce the radar cross section (RCS) of the enclosed antenna outside its operating band. [3]
- Making polarizers, for example, circular polarization (CP) are used in radar applications. The advantages of a CP over linear polarization (LP) is that it has lower susceptibility to the multi-path, atmospheric absorption and reflections effects. [4]

- To reduce the adjacent channel interference in the communication systems due to the congestion of the electromagnetic spectrum, several FSS structures like dipole, Jerusalem cross, ring, tripod, dross dipole and square loop have been developed [5]
- Filters for Earth Observation Remote Sensing Instruments by separating the scene radiation into separate frequency channels [6]. By providing frequency selective beam splitting in the feed train thus vastly reducing the size and mass of the antenna system and minimize the filter insertion loss[7] as shown in Figure 1.2.1.

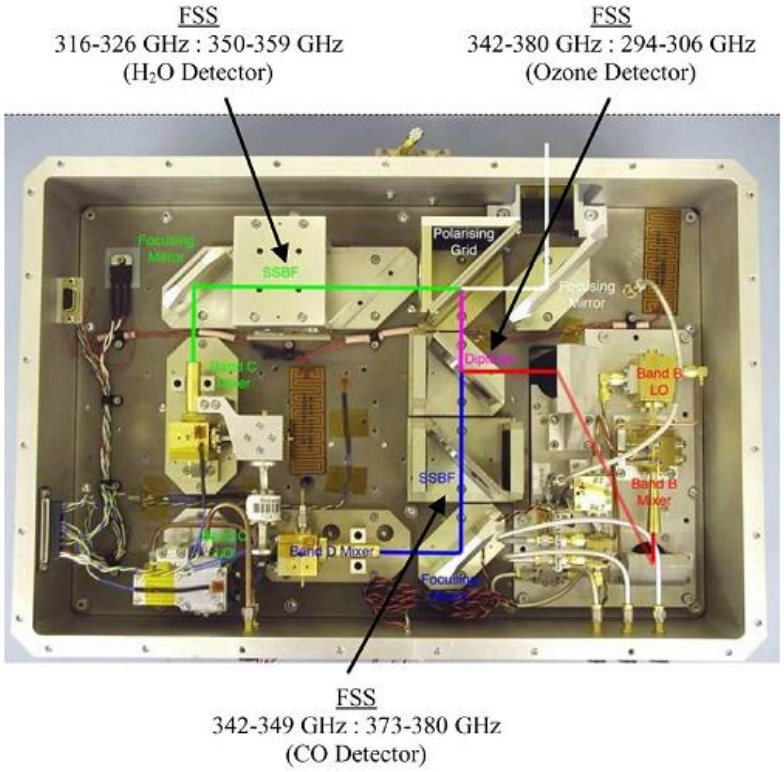

Figure 1.2: MARSCHALS quasi-optical feed train

One important application of selective surfaces is to shield the mobile signals for a variety of reasons that would make clear later, the following is an overview of the mobile networks

1.3 Generations of mobile communication systems

The generations of mobile communication systems are presented here since the main application

in the current thesis is to use FSS to block mobile signals. Mobile phone network has been historically divided into four generations, each generation has specific characteristics that distinguish it from other Each generation is different from the other in terms of frequency, data rate, maximum number of users and the geographical area covered by the network. The following is a brief explanation of each generation.

1.3.1 First generation of the network appeared in the 1980s and started with the advanced mobile phone service (AMPS) which has the below features [8,9,10]:

- Based on analog communications
- Support only voice transmissions
- Use frequency division multiple access (FDMA) with 30kHz for each channel
- The frequency is ranging from 824 MHz to 894 MHz
- Two 25 MHz band are allocated, one for upload frequency (from mobile unit to the base station) and other for download frequency (from base station to the mobile unit)

1.3.2 Second generation appeared in the 1990s and has the below features [11,12]:

- Based on digital communications
- Voice calls are becoming clearer and the communications are encrypted
- The Time Division Multiple access (TDMA) (Figure 1.3) -based Global System for Mobile (GSM) system and the Code Division Multiple Access (CDMA) (Figure 1.4) –based Interim Standard 95 (IS-95) system.
- Supported better voice and text transmissions.
- The frequency bands are 900 and 1800MHz
- The GSM Architecture is based on Gaussian Minimum Shift Keying (GMSK) scheme
- The GSM 900 system uses two 25-MHz bands for the uplink and downlink, and within this spectrum 200-KHz channels are allocated. The uplink and downlink are separated by a 45-MHz spacing. GSM 1800 uses two 75-MHz bands for the uplink and downlink. Again 200-KHz channels are allocated within those bands and are separated by a 95-MHz spacing. The 1900-MHz systems use two 60-MHz bands for the uplink and downlink using 200-KHz channels within those bands and separated

by 80-MHz spacing.

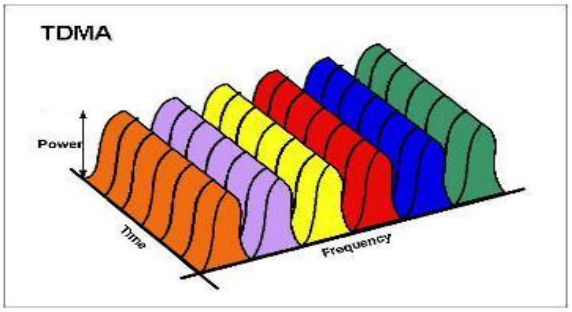

Figure 1.3: Time Division Multiple access

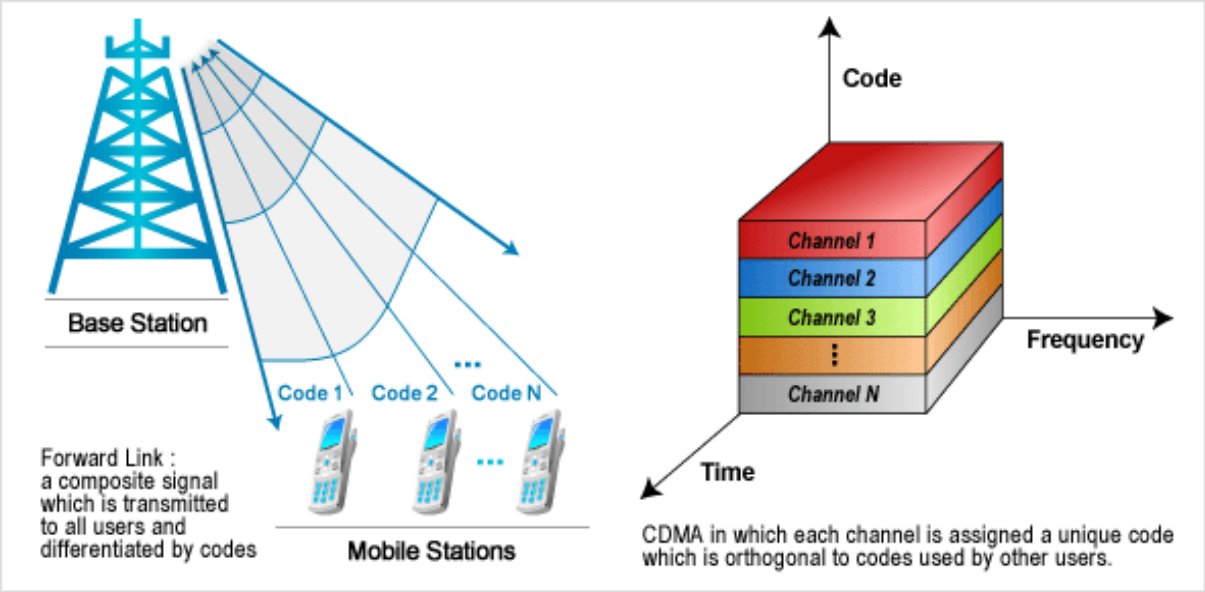

Figure 1.4: Code Division Multiple Access [13]

1.3.3 Third generation (3G)

This technology has greatly helped in the development of wireless services, which included voice telephony, mobile Internet access, fixed wireless internet access, video calls and mobile TV. 3G uses services and networks that comply with the International Mobile Telecommunications-2000 (IMT-2000) specifications.

The first 3G network was launched in May 2001 in a test release as Wideband Code Division Multiple Access (WCDMA) technology in Japan. The first Universal Mobile

Telecommunications System (UMTS) (based WCDMA) network was launched in Europe in December 2001.

The UMTS system, used primarily in Europe, Japan, China (however with a different radio interface) and other regions predominated by GSM 2G system infrastructure. The cell phones are typically UMTS and GSM hybrids. Several radio interfaces are offered, sharing the same infrastructure:

- The original and most widespread radio interface is called W-CDMA.
- The Time-Division Synchronous Code-Division Multiple-Access (TD-SCDMA) radio interface was commercialized in 2009 and is only offered in China.
- The latest UMTS release, High Speed Packet Access (HSPA+), can provide peak data rates up to 28 Mbit/s in the downlink and 22 Mbit/s in the uplink.

UMTS network using the CDMA2000 technology, first offered in 2002 in USA, used especially in North America and South Korea, sharing infrastructure with the IS-95 2G standard. The cell phones are typically CDMA2000 and IS-95 hybrids.[14]

3G network has the below features:

- Wider coverage area
- Improve spectral efficiency
- Greater network capacity
- More services include video calls and broadband wireless data
- Data rate reached 14.4 Mb/s on downlink and 5.8 Mb/s on uplink

2G / 3G Cellular terminology is illustrated in Table 1.1

Table 1.1: 2G / 3G Cellular Wireless data transport terminology [15]

Transport technology	Description	Typical use/Data transmission speed	Pros/cons
TDMA	Time Division Multiple Access is 2G technology	Voice and data Up to 9.6kbps	Low battery consumption, but transmission is one-way, and its speed pales next to 3G technologies
GSM	Global System for Mobile Communications is a 2G digital cell phone technology	Voice and data. This European system uses the 900MHz and 1.8GHz frequencies. In the United States it operates in the 1.9GHz PCS band Up to 9.6kbps	Popular around the globe. Worldwide roaming in about 180 countries, but GSM's short messaging service (GSM-SMS) only transmits one-way, and can only deliver messages up to 160 characters long
GPRS	General Packet Radio Service is a 2.5G network that supports data packets	Data Up to 115kbps; the AT&T Wireless GPRS network will transmit data at 40kbps to 60kbps	Messages not limited to 160 characters, like GSM SMS
EDGE	Enhanced Data GSM Environment is a 3G digital network	Data Up to 384kbps	May be temporary solution for operators unable to get W-CDMA licenses
CDMA	Code Division Multiple Access is a 2G technology developed by Qualcomm that is transitioning to 3G		Although behind TDMA in number of subscribers, this fast-growing technology has more capacity than TDMA
W-CDMA (UMTS)	Wideband CDMA (also known as Universal Mobile Telecommunications System--UMTS) is 3G technology. On November 6, 2002, NTT DoCoMo, Ericsson, Nokia, and Siemens agreed on licensing arrangements for W-CDMA, which should set a benchmark for royalty rates	Voice and data. UMTS is being designed to offer speeds of at least 144kbps to users in fast-moving vehicles Up to 2Mbps initially. Up to 10Mbps by 2005, according to designers	Likely to be dominant outside the United States, and therefore good for roaming globally. Commitments from U.S. operators are currently lacking, though AT&T Wireless performed UMTS tests in 2002. Primarily to be implemented in Asia-Pacific region
CDMA2000 1xRTT	A 3G technology, 1xRTT is the first phase of CDMA2000	Voice and data Up to 144kbps	Proponents say migration from TDMA is simpler with CDMA2000 than W-CDMA, and that spectrum use is more efficient. But W-CDMA will likely be more common in Europe
CDMA2000 1xEV-DO	Delivers data on a separate channel	Data Up to 2.4Mbps	(see CDMA2000 1xRTT above)
CDMA2000 1xEV-DV	Integrates voice and data on the same channel	Voice and data Up to 2.4Mbps	(see CDMA2000 1xRTT above)

1.3.4 Fourth generation:

The prerelease appeared in 2006 using Worldwide Interoperability for Microwave Access (WiMAX) technology, and the first release appeared in 2009 with Long Term Evolution (LTE) technology with the below features:

- Data rate up to 100Mbps for mobile users and up to 1Gbps for fixed stations
- High Capacity Systems.
- Quick response time systems.
- Support Voice Over Internet Protocol VoIP and data.
- Maximum 2G/3G spectrum reusability.
- High quality audio/video streaming over Internet Protocol (IP).

Table 1.2: (a) WiMAX Release 2.0 (802.16m) technical specifications, (b) LTE-Advanced technical specifications [16]

a) WiMAX release 2		**b) LTE advanced (Third Generation Partnership Project (3GPP) release 10)**	
Generation	4G	Generation	4G
Expected release	2011	Expected release	2011
Physical layer	Down Link (DL): Orthogonal Frequency Division Multiple Access (OFDMA)	Physical layer	DL: OFDMA
	Up Link (UL): OFDMA		UL: SCFDMA
Duplex mode	Time – and frequency division duplex (TDD & FDD)	Duplex mode	Time Division Duplexing (TDD) & Frequency Division Duplexing (FDD)
User mobility	Up to 350 kmph	User mobility	Up to 350 kmph
Coverage	Up to 50 km	Coverage	Up to 100 km
Channel bandwidth	5, 10, 20, 40 MHz	Channel bandwidth	Up to 100 MHz
Peak data rates	DL: > 350 Mbps (4 x 4 antennas)	Peak data rates	DL: 1 Gbps
	UL: > 200 Mbps (2 x 4 antennas) at 20 MHz FDD		UP: 300 Mbps
Spectral efficiency	DL: > 2.6 bps / Hz (2x2)	Spectral efficiency	DL: 30 bps / Hz
	UL: > 1.3 bps / Hz (1x2)		UL: 15 pbs / Hz
Latency	Link layer: < 10 ms	Latency	Link layer: < 5 ms
	Handoff: < 30 ms		Handoff: < 50 ms
VoIP capacity	< 30 user per sector / MHz (TDD)	VoIP capacity	< 80 user per sector / MHz (FDD)
Other qualities	Full IP – based architecture 3G compatible Quality Of Service (QoS) support	Other qualities	Full IP – based architecture 3G compatible QoS support

1.4 Global mobile subscribers and market share by technology:

Many studies have shown the growing global demand for the third and fourth generation systems, though the second generation systems still occupies the lead globally in terms of use. According to the "4gamericas" website, the percentage of networks that use the GSM technology in 2015 is 54% while the use of HSPA network reached 27.6% and LTE systems is 10.45% [17], as shown in Figure 1.5.

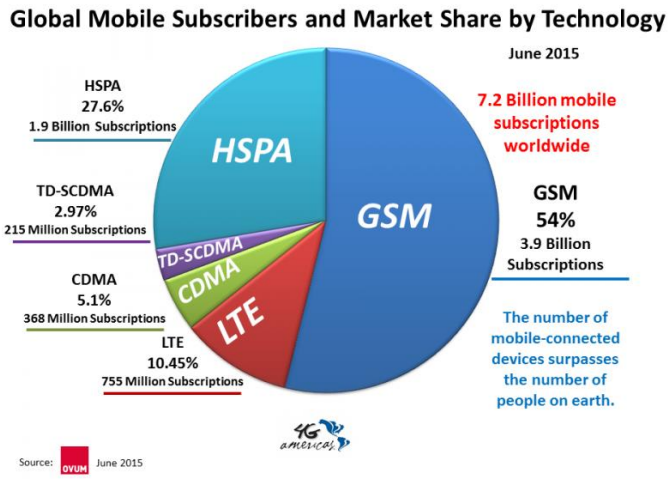

Figure 1.5: Global mobile subscribers and market share by technology

1.5 Frequency bands of generations:

1.5.1 Frequencies of GSM 900-1800 bands

GSM-900 and GSM-1800 are used in most parts of the world: Europe, Middle East, Africa, Australia, Oceania (and most of Asia) as shown in Figure 1.6.

GSM-900 uses 890–915 MHz to send information from the mobile station to the base station (uplink) and 935–960 MHz for the other direction (downlink), providing 124 RF channels (channel numbers 1 to 124) spaced at 200 kHz. Duplex spacing of 45 MHz is used. Guard bands 100 kHz wide are placed at either end of the range of frequencies. [18]

GSM-1800 uses 1,710 –1,785 MHz to send information from the mobile station to the base transceiver station (uplink) and 1,805–1,880 MHz for the other direction (downlink), providing

374 channels (channel numbers 512 to 885). Duplex spacing is 95 MHz. GSM-1800 is also called DCS (Digital Cellular Service) in the United Kingdom

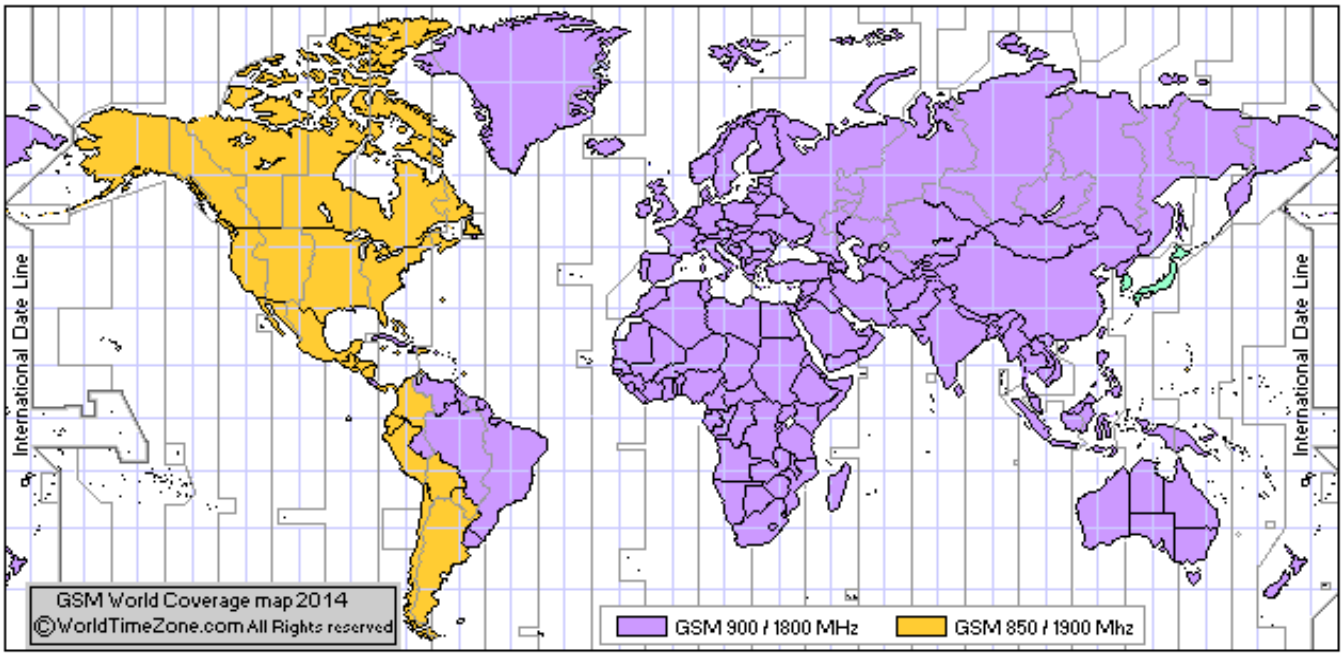

Figure 1.6: GSM (Group Special Mobile) - Global System for Mobile communications - most popular standard for phones in the world. GSM 900 / GSM 1800 MHz are used in most parts of the world: Europe, Asia, Australia, Middle East, and Africa. GSM 850 / GSM 1900 MHz are used in the United States, Canada, Mexico and most countries of S. America. [19]

1.5.2 Frequencies of 3G bands

The main UMTS / WCDMA frequency bands for FDD operation are summarized in table 1.3.

Table 1.3: 3G UMTS FREQUENCY BANDS – FDD [20]

3G UMTS FREQUENCY BANDS – FDD				
BAND NUMBER	BAND	COMMON NAME	UL FREQUENCIES	DL FREQUENCUES
1	2100	IMT	1920 - 1980	2120 - 2170
2	1900	PCS A-F	1850 - 1910	1930 - 1990
3	1800	DCS	1710 - 1785	1805 - 1880
4	1700	AWS A-F	1710 - 1755	2110 - 2155
5	850	CLR	824 - 849	869 - 894

6	800		830 - 840	875 - 885
7	2600	IMT-E	2500 - 2570	2620 - 2690
8	900	E-GSM	880 - 915	925 - 960
9	1700		1749.9 - 1784.9	1844.9 - 1879.9
10	1700	EAWS A-G	1710 - 1770	2110 - 2170
11	1500	LPDC	1427.9 - 1447.9	1475.9 - 1495.9
12	700	LSMH	699 - 716	729 - 746
13	700	USMH C	777 - 787	746 - 756
14	700	USMH D	788 - 798	758 - 768
19	800		832.4 - 842.6	877.4 - 887.6
20	800	EUDD	832 - 862	791 - 821
21	1500	UPDC	1447.9 - 1462.9	1495 - 1510.9
22	3500		3410 - 3490	3510 - 3590
25	1900	EPCS A-G	1850 - 1915	1930 - 1995
26	850	ECLR	814 - 849	859 - 894

Frequency bands 15, 16, 17, 18, 23 and 24 are now reserved frequency bands.

1.5.3 Frequencies of 4G Bands:

The LTE networks use two types of technology, FDD, TDD. The FDD use 2 frequencies one for uplink, other for downlink and between them there is a gap as shown in Figure 1.7. The gap must be sufficient to enable the roll-off of the antenna filtering to give sufficient attenuation of the transmitted signal within the receive band. [21]

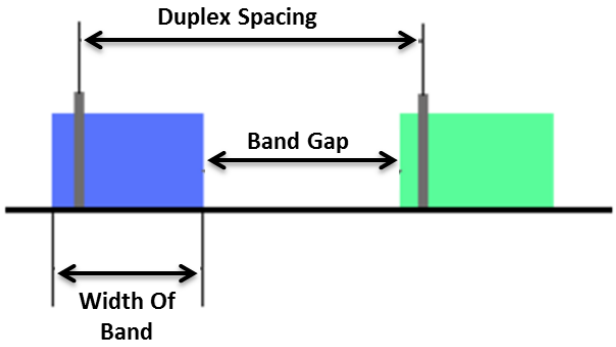

Figure 1.7 : frequencies separated by gap

The TDD uses the same frequency and being time multiplexed.

The LTE frequency band has been divided for many sub bands, and each band has a number. Currently the LTE bands between 1 & 22 are for paired spectrum, i.e. FDD, and LTE bands between 33 & 41 are for unpaired spectrum, i.e. TDD. [21]. Table 1.4 shows the FDD LTE bands, while Table 1.5 shows the TDD LTE bands.

Table 1.4: FDD LTE bands and frequencies

FDD LTE BANDS & FREQUENCIES					
LTE BAND NUMBER	UPLINK (MHZ)	DOWNLINK (MHZ)	WIDTH OF BAND (MHZ)	DUPLEX SPACING (MHZ)	BAND GAP (MHZ)
1	1920 - 1980	2110 - 2170	60	190	130
2	1850 - 1910	1930 - 1990	60	80	20
3	1710 - 1785	1805 -1880	75	95	20
4	1710 - 1755	2110 - 2155	45	400	355
5	824 - 849	869 - 894	25	45	20
6	830 - 840	875 - 885	10	35	25
7	2500 - 2570	2620 - 2690	70	120	50
8	880 - 915	925 - 960	35	45	10
9	1749.9 - 1784.9	1844.9 - 1879.9	35	95	60
10	1710 - 1770	2110 - 2170	60	400	340
11	1427.9 - 1452.9	1475.9 - 1500.9	20	48	28
12	698 - 716	728 - 746	18	30	12
13	777 - 787	746 - 756	10	-31	41
14	788 - 798	758 - 768	10	-30	40
15	1900 - 1920	2600 - 2620	20	700	680
16	2010 - 2025	2585 - 2600	15	575	560
17	704 - 716	734 - 746	12	30	18
18	815 - 830	860 - 875	15	45	30
19	830 - 845	875 - 890	15	45	30
20	832 - 862	791 - 821	30	-41	71
21	1447.9 - 1462.9	1495.5 - 1510.9	15	48	33

FDD LTE BANDS & FREQUENCIES					
LTE BAND NUMBER	UPLINK (MHZ)	DOWNLINK (MHZ)	WIDTH OF BAND (MHZ)	DUPLEX SPACING (MHZ)	BAND GAP (MHZ)
22	3410 - 3500	3510 - 3600	90	100	10
23	2000 - 2020	2180 - 2200	20	180	160
24	1625.5 - 1660.5	1525 - 1559	34	-101.5	135.5
25	1850 - 1915	1930 - 1995	65	80	15
26	814 - 849	859 - 894	30 / 40		10
27	807 - 824	852 - 869	17	45	28
28	703 - 748	758 - 803	45	55	10
29	n/a	717 - 728	11		
30	2305 - 2315	2350 - 2360	10	45	35
31	452.5 - 457.5	462.5 - 467.5	5	10	5

Table 1.5: TDD LTE bands and frequencies

TDD LTE BANDS & FREQUENCIES		
LTE BAND NUMBER	ALLOCATION (MHZ)	WIDTH OF BAND (MHZ)
33	1900 - 1920	20
34	2010 - 2025	15
35	1850 - 1910	60
36	1930 - 1990	60
37	1910 - 1930	20
38	2570 - 2620	50
39	1880 - 1920	40
40	2300 - 2400	100
41	2496 - 2690	194
42	3400 - 3600	200
43	3600 - 3800	200
44	703 - 803	100

1.6 Thesis objective

Nowadays we need to prevent some signals entering some areas. For example in intensive care rooms in hospitals we must prevent mobile calls without using jammers, and so places of worship, prisons, secured meeting rooms, and other places.

In this research we intend to design a frequency selective surface (FSS) to achieve this goal. The circuit will be designed using microstrip technology on printed circuit board that can be mounted on a wall and wire net that can be built in open areas. The signals of interest here to be blocked is the downlink bands of multi cellular networks that are used in Historical Palestine. [22],[23]

Bands that will be covered through the research are:

- GSM signal (925-960 MHz), (1805-1880 MHz).
- 3G mobile network (2110-2170 MHz).
- Band 7 of LTE systems (2620 – 2690 MHz).

1.7 Thesis overview:

The thesis consists of four chapters

The first chapter briefly reviewed the different generations of mobile phone networks and the most important characteristics and also the global ranges for each generation. Also the most important applications of the FSS technique are presented.

In the second chapter the theoretical background of the frequency selective surfaces (FSS) and the most important designs used will be presented. Moreover, mathematical equations for some known FSS structures are presented.

In the third chapter some researches and designs published in literature on the subject of the thesis will be introduced, and also four FSS designs along with their will be presented.

Chapter four shows the conclusions drawn from the current work in addition to future work.

Chapter 2: Frequency Selective Surface Theory

Frequency Selective Surfaces are a periodic structures etched in a dielectric surface or a group of metallic structures in vacuum. These shapes are resonant with some frequencies depending on lengths and type of materials, and the selective surfaces work as band pass or band stop filters depending on type of metallic elements patch or aperture. The patch element array behaves as a band stop filter and the aperture element array acts as a band pass filter as shown in Figure 2.1 [24].

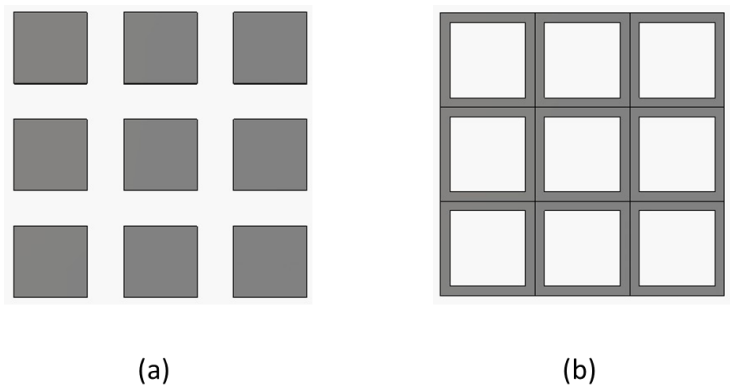

Figure 2.1: (a) patch elements, (b) aperture elements

Many factors are involved in understanding the operation and application of frequency selective surfaces. These include analysis techniques, operating principles, design principles, manufacturing techniques and methods for integrating these structures into space, ground and airborne platforms. The overall frequency response including its bandwidth and dependence on the incidence angle and polarization is determined by the element geometry and the substrate parameters. [25]

2.1 The relevant concepts in electromagnetic theory

To understand the underlying mechanism on which the filters function. As shown in Figure 2.2, an incident plane wave strikes the filter and causes the electrons in the metal to oscillate. If a large portion of the incident energy is absorbed by these electrons they re-radiate and cancel the initial field, causing the transmittance through the filter to be low. In this case, the

electrons will re-radiate toward the left and cause the reflected wave amplitude to be high. If only a small portion of the incident power is absorbed no such cancellation occurs and the transmittance will be high. In general the transmittance through the filter is a function of frequency; in other words, the electrons in the metal will absorb and re-radiate some wavelengths with higher efficiency than others. The shape of the transmittance curve depends on the pattern etched into the metal filter, and we can etch various patterns into our metal to obtain filters of varying behavior. [26]

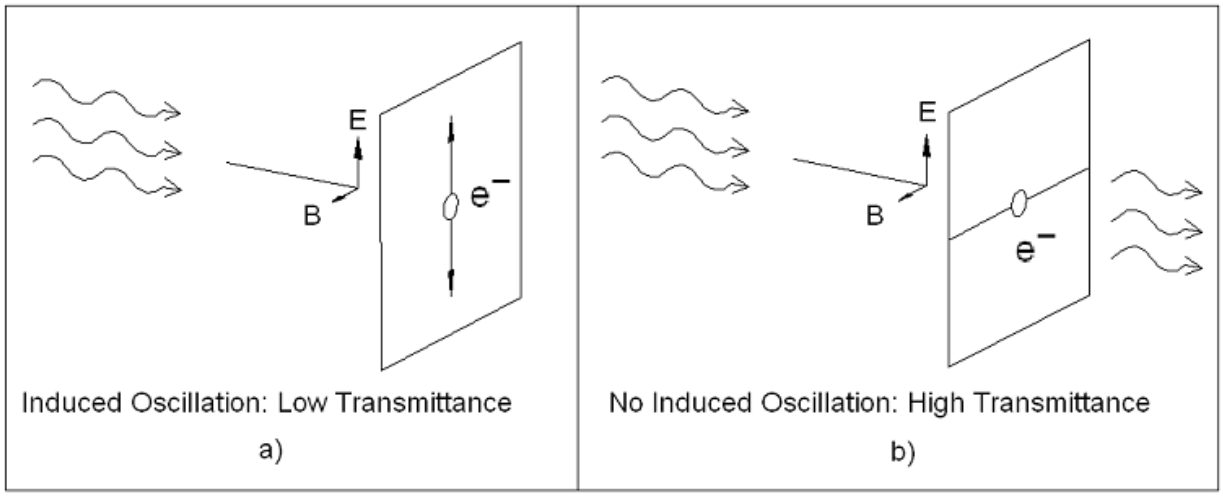

Figure 2.2: (a) Electron in filter plane undergoes oscillations driven by source wave, (b) Electron constrained to move along wire cannot undergo oscillations.

2.2 Filter Geometries and Equivalent Circuits:

Although the simulation software analyzes the geometries we design accurately, we often need to understand the physical background behind the geometries in which we design. The most common shapes used in FSS and their equivalent circuits and mathematical analysis are presented here.

The three most common types of filters are: strip grating filters, mesh filters, and cross-mesh filters. The first type is used to illustrate the theoretical idea of filter, the second type is useful because of their polarization-independence property, and the third type that we are interested in is used as band-pass and band-stop filters.

2.3 Strip Grating Filters:

The geometry of the strip grating filter is shown in Figure 2.3 [26]. If the E-field is parallel to the metal strips we have an inductive strip-grating filter as shown in Figure 2.4 (left); if the E-field is perpendicular to the strips we have a capacitive strip-grating filter as shown in Figure 2.4 (right).

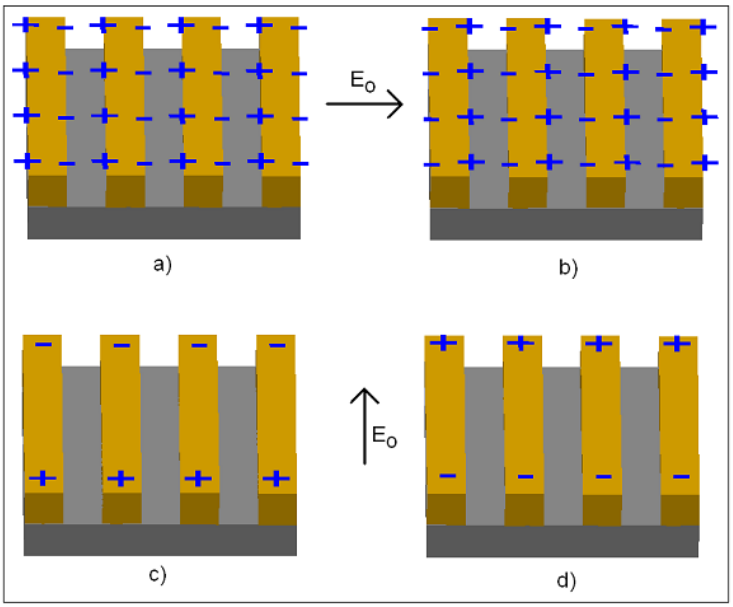

Figure 2.3: If the E-field is perpendicular to the strips the filter switches between states a and b, if it is parallel to the strip the filter switches between c and d.

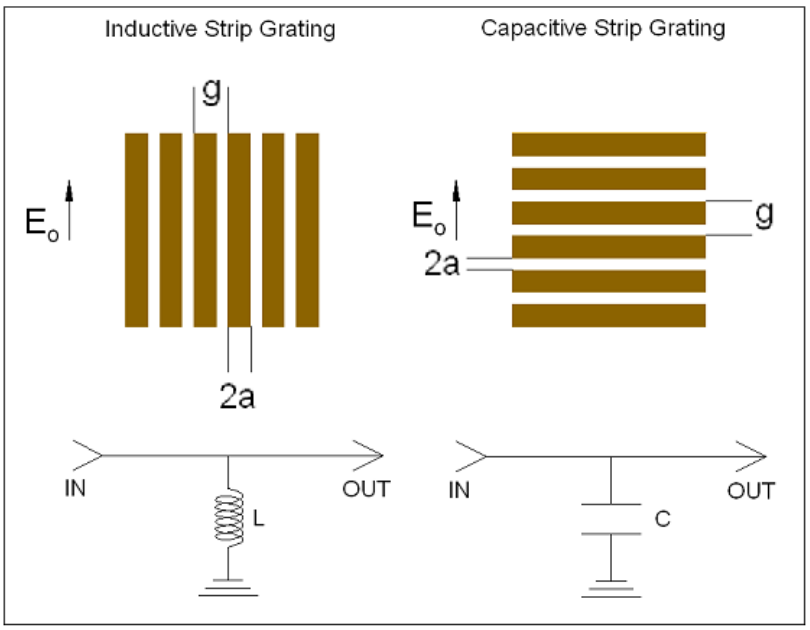

Figure 2.4: strip-grating filters and its equivalent circuit

Modeling arrays at oblique angles of incidence therefore requires expressions for the admittances for both transverse electric (TE) and transverse magnetic (TM) incidence.

TM-incidence occurs when the E-field is polarized parallel to the plane of incidence, i.e. θ = 0°, and TE-incidence when the E-field is perpendicular to the plane of incidence, i.e. Φ = 0° [27]. Using the geometry of Figure 2.5, for conductors of periodicity p, width w, and spaced a distance g, Marcuvitz gave normalized admittance expressions for two cases [28]:

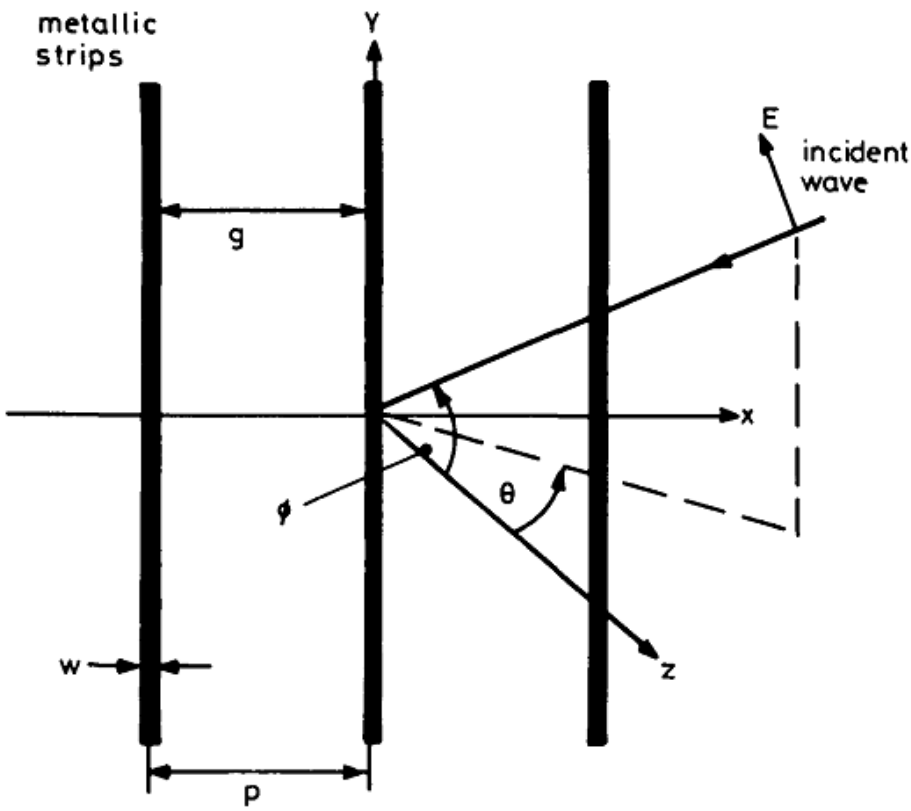

Figure 2.5: Plane wave incident on an inductive strip grating, for a capacitive strip grating exchange the incident electric field E for a magnetic field H

The normalized shunt inductive reactance expression of the inductive strip grating was given by Marcuvitz as:

$$X_{TE} = w.\frac{L}{Z_O} = p.\frac{\cos\theta}{\lambda}.(\ln\left(cosec\left(\frac{\pi w}{2p}\right)\right) + G(p, w, \lambda, \theta)) \tag{2.1}$$

The normalized shunt susceptance expression of the capacitive strip grating was given by Lee as:

$$B_{TE} = w.\frac{C}{Y_O} = 4p.\frac{sec\,\theta}{\lambda}.(ln\left(cosec\left(\frac{\pi g}{2p}\right)\right) + G(p,w,\lambda,\theta)) \tag{2.2}$$

Where G is the correction term given as:

$$G(p,w,\lambda,\theta) = 0.5\frac{(1-\beta^2)^2\left[\left(1-\frac{\beta^2}{4}\right)(A_{1+}+A_{1-}) + 4\beta^2 A_{1+}A_{1-}\right]}{\left(1-\frac{\beta^2}{4}\right) + \beta^2(1+\frac{\beta^2}{2}-\frac{\beta^4}{8})(A_{1+}+A_{1-}) + 2\beta^6 A_{1+}A_{1-}} \tag{2.3}$$

$$A_{1\pm} = \frac{1}{\sqrt{(\frac{p\,sin\,\theta}{\lambda} \pm 1)^2 - p^2/\lambda^2}} - 1 \tag{2.4}$$

$$\beta = sin(\frac{0.5\pi w}{p}) \tag{2.5}$$

These equations are valid for wavelength and angles of incident θ in the range $\boldsymbol{p(1+\sin\theta)/\lambda < 1}$

2.4 Mesh Filters:

As shown in Figure 2.6, the capacitive mesh consists of a grid of metal squares while the inductive mesh represents the complementary structure. These filters will also behave as low-and high-pass filters but have the additional advantage that the transmittance through the filter is independent of the polarization of the source [26].

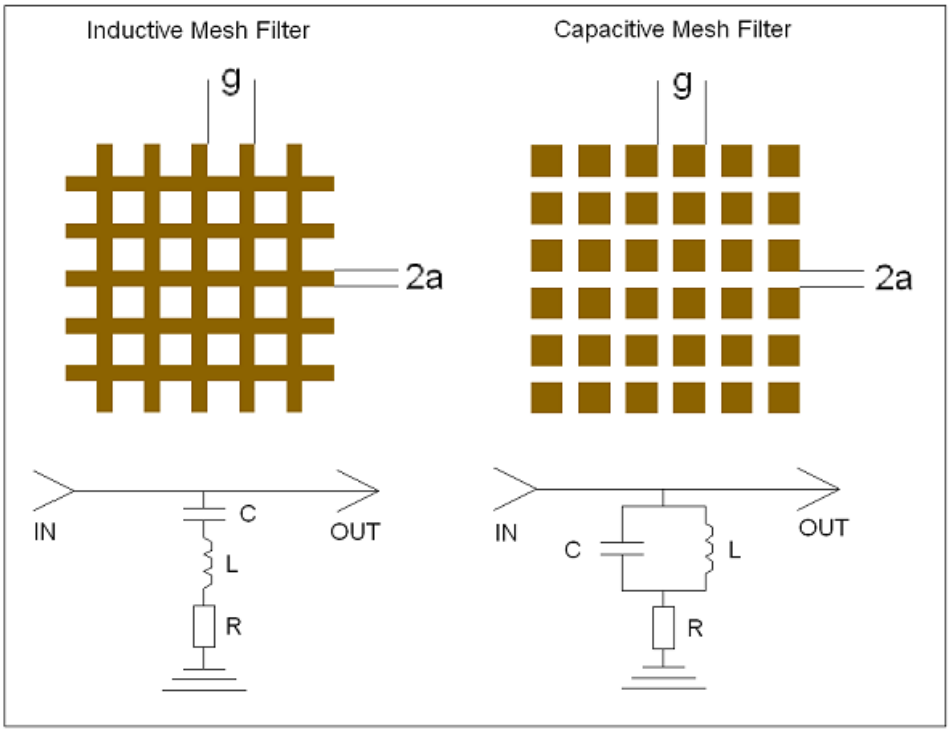

Figure 2.6: mesh filters and its equivalent circuit

The capacitive mesh filter has a transmission zero at frequency f=c/g, where c is the speed of the light. At frequencies above this critical frequency the transmission begins to rise steadily. The steepness of the curve depends on the ratio a/g, with a higher ratio leading to a steeper curve. The inductive mesh filter has full transmission at frequency f=c/g, and the transmission begins to drop above this frequency. The steepness of the curve is again determined by the ratio a/g.

2.5 Cross-Mesh Filters:

These filters are similar to mesh filters except that the repeated grid element is a cross instead of a square. The dimensions of these crosses determine a resonant wavelength. The resonant wavelength has a transmission zero (Band Stop Filter) for capacitive cross-mesh filters and has full transmission (Band Pass Filter) for inductive cross-mesh filters as shown in Figure 2.7 [26].

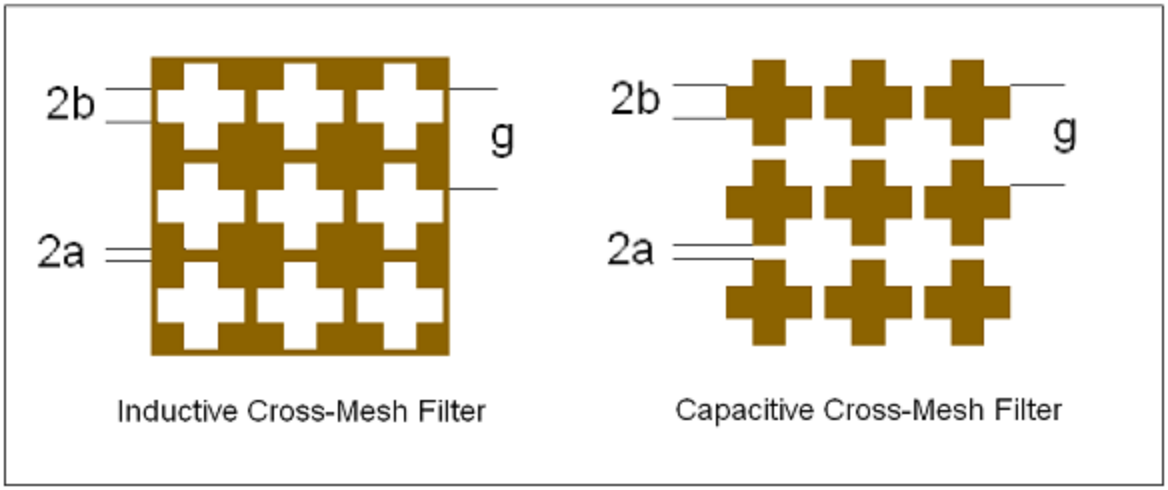

Figure 2.7: cross-mesh filters

Increasing the length of the crosses reduces the resonant frequency. Increasing the width of the crosses increases the bandwidth and increases the resonant frequency slightly. Increasing the substrate thickness decreases the resonant frequency slightly. Rounding the corners of the crosses increases the resonant frequency. Increasing the center-to-center spacing of the crosses decreases the bandwidth. [26]

2.6 Analysis of More complex structures:

2.6.1 Square Loop FSS:

The frequency characteristic of Square Loop FSS's has a single reflection band and a lower-frequency transmission band which can be approximately represented with resonant circuits consisting of inductances and capacitances via the Equivalent Circuit Model [29].

In the FSS model, the array is represented by a single series LC circuit shunted across a transmission line of impedance Z_o as shown in Figure 2.8 (b), where Z_o is the characteristic impedance of free space. Values for L and C are determined later.

Figure 2.8 (a) shows an infinite thin array of narrow continuous perfectly conducting strips of period p and width w and Figure 2.8 (b) is the equivalent circuit of it [29].

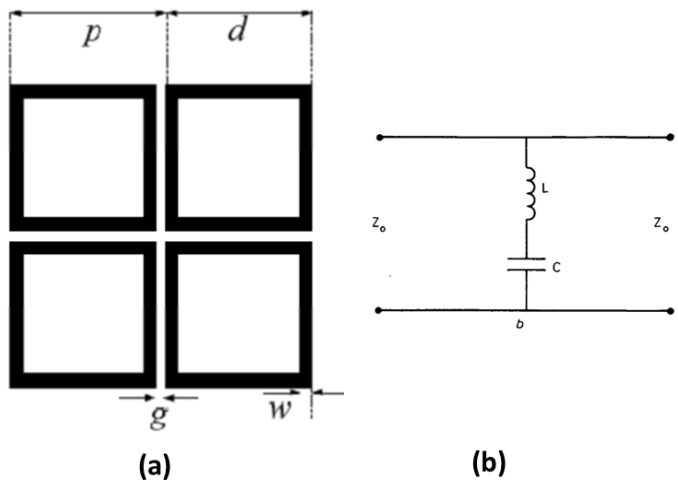

Figure 2.8: a) Layout of square loop arrays, b) Equivalent circuit

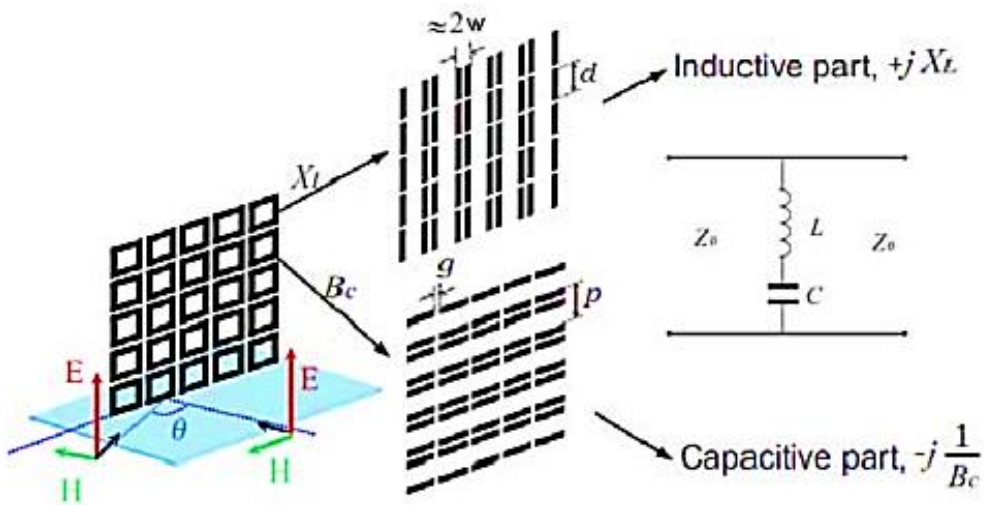

Figure 2.9: analysis of square loop FSS

The normalized shunt inductive reactance expression of the square loop FSS is [29]

$$X_{TE} = F(p, 2w, \lambda) \tag{2.6}$$

$$X_{TE} = w.\frac{L}{Z_O} = p.\frac{\cos\theta}{\lambda}.(ln\left(cosec\left(\frac{2\pi w}{2p}\right)\right) + G(p, w, \lambda, \theta)) \tag{2.7}$$

G is obtained from eq. 2.3

$$X_{TM} = p.\frac{sec\,\emptyset}{\lambda}.(ln\left(cosec\left(\frac{2\pi w}{2p}\right)\right) + G(p, w, \lambda, \emptyset)) \tag{2.8}$$

The normalized shunt susceptance expression of the capacitive strip grating

$$B_{TM} = 4F(p, g, \lambda) = 4p.\frac{cos\,\emptyset}{\lambda}.(ln\left(cosec\left(\frac{\pi g}{2p}\right)\right) + G(p, g, \lambda, \emptyset)) \tag{2.9}$$

$$B_{TE} = w.\frac{C}{Y_O} = 4p.\frac{sec\,\theta}{\lambda}.(ln\left(cosec\left(\frac{\pi g}{2p}\right)\right) + G(p, w, \lambda, \theta)) \tag{2.10}$$

The surface impedance of FSS is

$$\boldsymbol{Z = jwL + \frac{1}{jwC} = j(wL - \frac{1}{wC})} \tag{2.11}$$

The reflection coefficient is [30]

$$S_{11} = -\frac{1}{\frac{2Z}{Z_o} + 1} \tag{2.12}$$

For square loop FSS etched into dielectric substrate, the equivalent circuit is shown in Figure 2.10 [31].

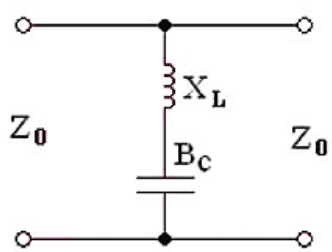

Figure 2.10: equivalent circuit for square loop

The Inductive reactance element is calculated as in eq.2.13

$$\frac{X_f}{Z_o} = \frac{1}{\sqrt{\varepsilon_e}} . \frac{d}{p} . F(p, 2w, \lambda_e) \tag{2.13}$$

F is obtained from eq.2.6

And the capacitance reactance element is calculated as in eq.2.14

$$B_f . Z_o = \frac{4d}{p} . \sqrt{\varepsilon_e} F(p, g, \lambda_e) \tag{2.14}$$

The effective wavelength

$$\lambda_e = \lambda / (\boldsymbol{\varepsilon_e})^{-0.5} \tag{2.15}$$

The effective permittivity is given by

$$\varepsilon_e = \frac{\varepsilon_r + 1}{2} + \frac{\varepsilon_r - 1}{2} . \frac{1}{\sqrt{1 + \frac{12t}{w}}} \tag{2.16}$$

Where t is the thickness of substrate and ε_r is the permittivity of dielectric

It can be seen that the impedance X_f/Z_o is reduced by a factor d/p. A thin dielectric substrate, on which the conductive elements are printed, causes an increase in the susceptance $(B_f . Z_o)$ of the array while no effect on the inductive reactance is observed. [32]

2.6.2 Jerusalem Cross:

Jerusalem Cross is one of the other well-known forms, where there are a number of computational analysis to calculate the frequency and bandwidth to be achieved.

Assuming a vertically polarized wave is normally incident on the grid, Leonard and Cofer developed an equivalent circuit model for the Jerusalem cross, consisting of a combination of two LC resonant circuits in series, as illustrated in Figure 2.11, 2.12 [33]

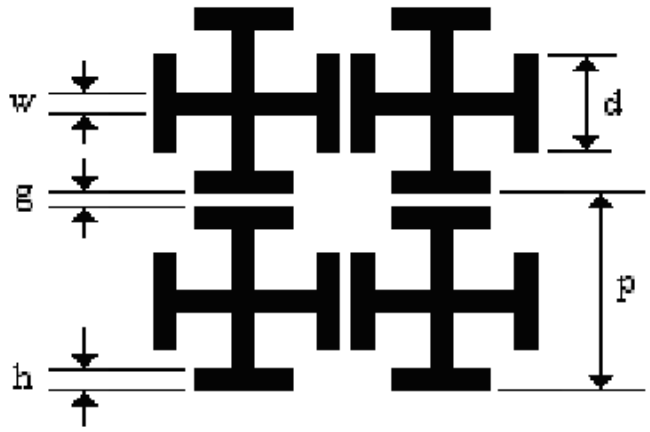

Figure 2.11: Jerusalem cross periodic array

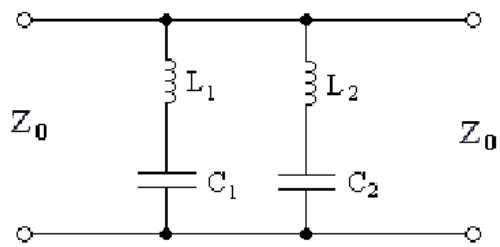

Figure 2.12: equivalent circuit of Jerusalem cross

Figure 2.13 shows the frequency response of Jerusalem cross FSS

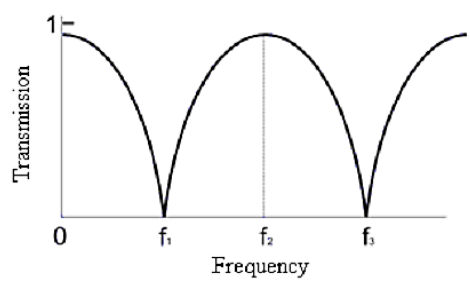

Figure 2.13: frequency response of Jerusalem cross

The value of each inductive strip X_L of width w is calculated using

$$\frac{X_L}{Z_O} = F(p, w, \lambda, \emptyset) = p.\frac{\cos \emptyset}{\lambda}.(ln\left(cosec\left(\frac{\pi w}{2p}\right)\right) + G(p, w, \lambda, \emptyset)) \quad (2.17)$$

The susceptance $B_1 = B_d + B_g$, where B_g is due to capacitance between the final horizontal arms, spaced by g, reduced by a factor of d/p

$$B_g = \frac{4d}{p}.F(p, g, \lambda) \tag{2.18}$$

The susceptance B_g is between final vertical capacitors spaced by (p-d) and it is calculated as:

$$B_d = \frac{4(2h + g)}{p}.F(p, p - d, \lambda) \tag{2.19}$$

The inductive reactance X_{L2} is calculated as:

$$\frac{X_{L2}}{Z_o} = \frac{d}{p}.F(p, 2w, \lambda, \theta) \tag{2.20}$$

The value of C_2 is not calculated directly using the analysis as described before, but from the assumption of a dipole resonance with the frequency f_3, so $\lambda_3 = \frac{\mathrm{d}}{0.43}$, then f_3 is calculated as:

$$f_3 = \frac{1}{2\pi\sqrt{L_2 C_2}} \tag{2.21}$$

Reference [34] presented analysis for Jerusalem cross etched in dielectric slab with permittivity ε_r as shown in Figure 2.14 [34]

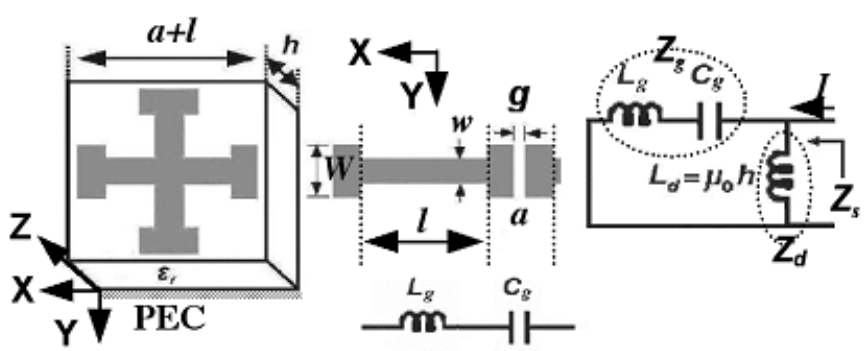

Figure 2.14: Jerusalem cross etched in dielectric slab

Where Z_d referred to the impedance of the perfect electric conductor (PEC) - backed dielectric slab, and Z_g is the grid impedance of the FSS.

2.7 A brief of most common FSS geometries

Table 2.1 illustrates a brief of most common FSS geometries [35].

Table 2.1: a brief of most common FSS geometries and its equivalent circuits

S. No	FSS	Circuit	Equivalent Circuit	Equivalent Inductance	Equivalent Capacitance
1	Single Square Loop	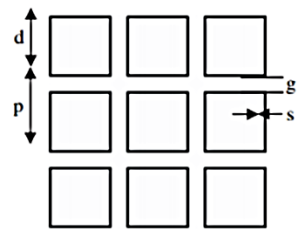	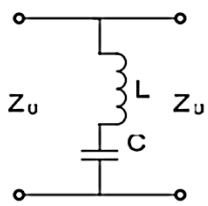	$\frac{X_L}{Z_0} = \frac{d}{p} F(p, 2s, \lambda)$	$\frac{B_c}{Z_0} = 4\frac{d}{p} F(p, g, \lambda)$
2	Double Square Loop	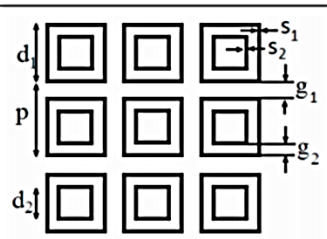	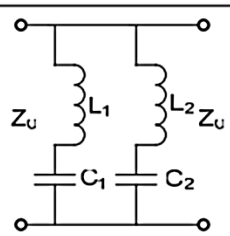	$\left(\frac{X_L}{Z_0}\right)_1 = F(p, s_1, \lambda)$ $\left(\frac{X_L}{Z_0}\right)_2 = F(p, s_2, \lambda)$	$\left(\frac{B_c}{Z_0}\right)_1 = 4F(p, g_1, \lambda)$ $\left(\frac{B_c}{Z_0}\right)_2 = 4F(p, g_2, \lambda)$
3	Triple Square Loop	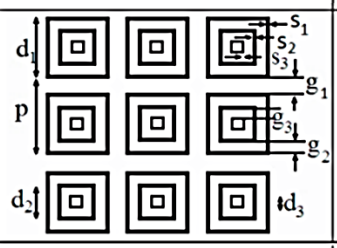	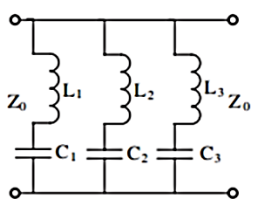	$\left(\frac{X_L}{Z_0}\right)_1 = F(p, s_1, \lambda)$ $\left(\frac{X_L}{Z_0}\right)_2 = F(p, s_2, \lambda)$ $\left(\frac{X_L}{Z_0}\right)_3 = F(p, s_3, \lambda)$	$\left(\frac{B_c}{Z_0}\right)_1 = 4F(p, g_1, \lambda)$ $\left(\frac{B_c}{Z_0}\right)_2 = 4F(p, g_2, \lambda)$ $\left(\frac{B_c}{Z_0}\right)_3 = 4F(p, g_3, \lambda)$
4	Cross Dipole	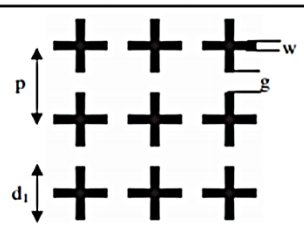	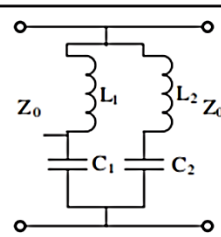	$\frac{X_L}{Z_0} = \frac{d}{p} F(p, w, \lambda_r)$	$B_g = 4\frac{w}{p} F(p, g, \lambda)$ $B_d = 4\frac{d}{p} F(p, p\text{-}w, \lambda)$
5	Jerusalem Cross Array	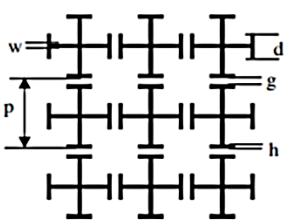	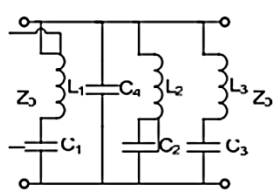	$\frac{X_L}{Z_0} = (\frac{d}{p}) F(p, w, \lambda)$	$B_d = 4\frac{(2h+g)}{p} F(p, p\text{-}d, \lambda)$ $B_g = 4\frac{d}{p} F(p, g, \lambda)$

2.8 Literature review

In [36], a square loop FSS structure (7×7) is designed and simulated at 2.4 GHz. The two materials of dielectric substrate which are FR4 board and glass have been used to produce hybrid materials. Six types of hybrid configurations have been studied . The results show that the return loss and transmission signal are effected by using hybrid materials which led to the compact structure. The disadvantage of this design that it covers only one band.

In [37], FSSs are deployed to selectively confine radio propagation in indoor areas, by artificially increasing the radio transmission loss naturally caused by building walls. FSS can also be used to channel radio signals into other areas of interest. Simulations and measurements have been carried out in order to verify the frequency selectivity of the FSS. Practical considerations regarding the deployment of FSS on building walls and the separation distance between the FSS and the supporting wall have been also investigated. A controlled, small-scale indoor environment has been constructed and measured in an anechoic chamber in order to practically verify this approach through the usage of ray tracing techniques.

The results suggest that proper FSS deployment can be used in indoor wireless environments in order to increase or restrict coverage and that Ray Tracing techniques can be applied to predict radio propagation in such environments. Proper FSS deployment can assist signal channeling or confine coverage in specific areas. The disadvantage of this design that the cell size is large and it covers only one band.

In [38], Frequency Selective Surface (FSS) is used as a sub reflector in a satellite. The FSS is designed by cutting slots in the square patch keeping same periodicity throughout. Frequency-selective surfaces are spatial filters which when incorporated as either flat or curved sub reflectors into a reflector antenna allows it to operate at a number of different frequency bands. This designed FSS structure has a wide stop band from 3.70GHz to 6.23GHz with percentage bandwidth of 51. Size reduction up to 83% is also achieved.

In [39], A simple and fast approach to design a thin and wideband radar absorbing structure is presented. The proposed method is applicable for design of an absorber consisting of any number of layers and any types of FSS, together with any given material that will be used for layer separation. An example of Radar Absorbing Material (RAM) designed by using the proposed methodology is also presented. The given RAM is a two layered structure backed by a ground plane. The layers are consisting of resistive FSS patterns, namely square ring and crossed dipole. Simulation results carried out by the high frequency structural simulator (HFSS) tool showed that the proposed approach is a good

candidate for designing thin and wideband radar absorbing structures. But this design is unstable at oblique incidences.

In [40], A series of novel miniaturized frequency selective surfaces consist of combinations of rectangle spiral-based elements are proposed. The simulation results show that using rectangle spiral-based structures instead of the meander line FSS provides at least 56% reduction of resonant frequencies. Moreover, the novel FSSs have excellent angle stability and polarization stability. Accordingly, the novel miniaturized FSSs have great potential for practical applications in limited space. But the transmission coefficient reduced about 20dB.

In [41], It has been shown that a bandpass FSS can be designed simply by using lumped reactive components. The full design methodology has been presented, resulting in the potential to design FSS with unit cell sizes. It has been shown that the resonant frequency can be controlled with the choice of lumped component values and to some extent the path length between the components. For practical designs the values of components will be available in discrete steps, however, fine tuning of the resonant frequency can be achieved by changing the path length. The effect of the resistance associated with the components has been evaluated and can be minimized by maximizing L/C and the path length between the components. The oblique incidence performance of the FSS is stable for both polarizations and methods for maintaining transmission loss at an acceptable level have been presented. This technology can be applied to low frequency radome and antenna applications, where physical volume is limited. The disadvantage of this design that it covers only one band.

In [42], Frequency selective shielding of a room at the most used communication bands of GSM 900 MHz, 1800 MHz and 2400 MHz is designed using Jerusalem cross elements. Minimum of 20 dB of shielding is achieved at the above bands. The designed tri-band band-stop filter has stable frequency response for varying incidence angles and polarization, which is the important requirement. The factors influencing the resonance frequency and bandwidth are also discussed. But the designed model may be not practical with 3G and LTE networks.

In [43], The shielding effectiveness of frequency selective surfaces (FSS) with double square elements reflecting at 900 MHz and 1800 MHz are analyzed using modal expansion techniques. It has been shown that the shielding effectiveness of the structure is greater than 60 dB at 900 MHz and greater than 40 dB at 1800 MHz. But the designed model may be not practical with 3G and LTE networks.

Chapter 3: Designs and simulations of Frequency Selective Surfaces

3.1 Introduction

Many designs adopted basically on popular models such as square loop, Jerusalem cross and triple poles to work the FSS. The problem in these designs the limited bands that can be covered in one design. This reason led to the innovation of many new shapes in two and three dimensions in order to achieve multi bands and minimize the size of the model.

3.2 Designs and simulations:

3.2.1 Goals of designs:

The circuit will be designed using microstrip technology on printed circuit board that can be mounted on a wall, and wire net that can be built in open areas. The signal of interest here to be blocked is the downlink bands for multi cellular networks that are used in Historical Palestine [18], [19].

Frequency Bands that are considered in the designs here are:

- GSM signal (925-960 MHz), (1805-1880 MHz).
- 3G mobile network (2110-2170 MHz).
- Band 7 of LTE systems (2620 – 2690 MHz).

3.2.2 Simulation Software CST:

The designs and simulations in this project are based on the Computer Simulation Technology (CST) Microwave Studio Suite which is a high performance electromagnetic simulation software [44]. There are two basic solver modules provided: time domain solver and frequency domain solver. The two solvers are totally different. Time domain solver is used for non-resonant structures and frequency domain solver contains alternatives for highly resonant structures. Besides frequency domain solver has the option of utilizing tetrahedral mesh that can discrete the structure better which is not available within time domain solver. In addition, time domain solver is only for normal incidence but frequency domain solver can be used for off-normal incidences. Because of the above I used the frequency domain solver to simulate designs.

3.3 Basics of the designs:

Designs are mainly based on the shapes of square loop and Jerusalem cross, some modifications are added to achieve the desired resonances. After that, some of the designs were not stable with varying the polarization so the rotation of the shapes four times clockwise occurred to solve this problem.

3.4 Bandstop double square loop FSS:

3.4.1 Structure of FSS:

The unit cell dimensions of bands top FSS are shown in Figure 3.1. The bandstop characteristics are achieved by designing two square-loop elements of different dimensions on FR-4 substrate. The thickness of FR-4 substrate is 1.6 mm aand relative permittivity (ε_r) and the loss tangent (tan δ) are 4.3 and 0.02, respectively. The periodicity of unit cell is 81.5×81.5 mm^2 . The circumference of the outer square-loop element is 278 mm which is tuned to 900 MHz while the circumference of the inner square loop element is 209 mm which is tuned to 1800 MHz. The width of both square loop elements is 5.8 mm. The dimensions of the FSS structure are depicted in Table 3.1.

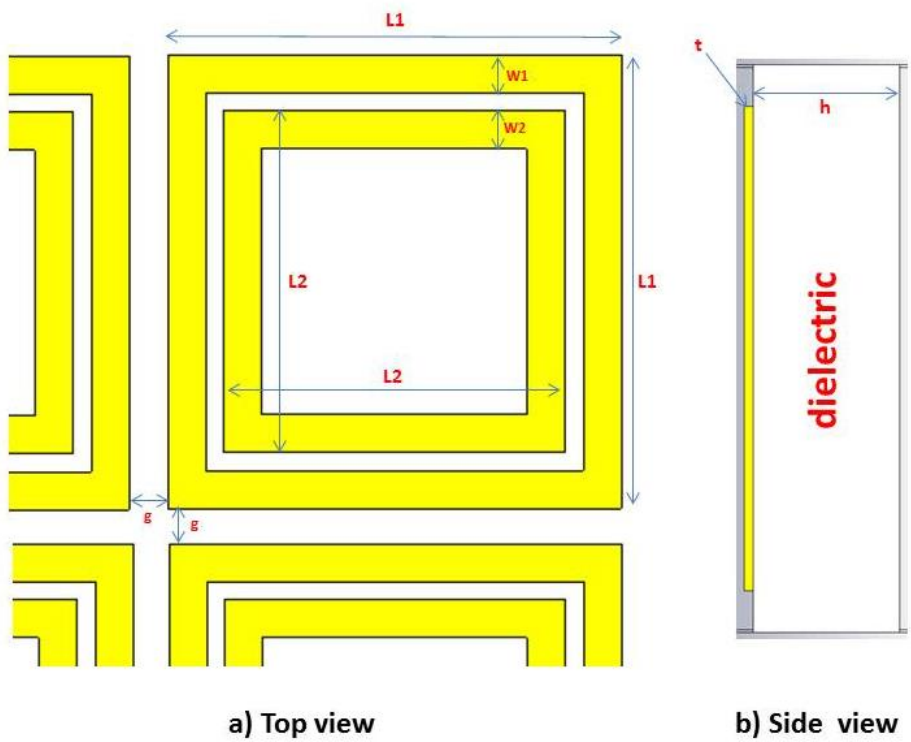

Figure 3.1: a) dimensions of square loop FSS, b) side view of the model

Table 3.1: dimensions of the design

Name	L1	L2	W1	W2	g	h	εr	t
Value (mm)	**69.5**	**52.25**	**5.8**	**5.8**	**12**	**1.6**	**4.3**	**0.1**

3.4.2 Simulation results:

The unit cell of FSS which is shown in Figure 3.2 is simulated by applying periodic boundary conditions using CST Microwave Studio, commercially available electromagnetic software. The transmission and reflection coefficients are obtained from 400-4000 MHz for both TM and TE polarizations at oblique incidences.

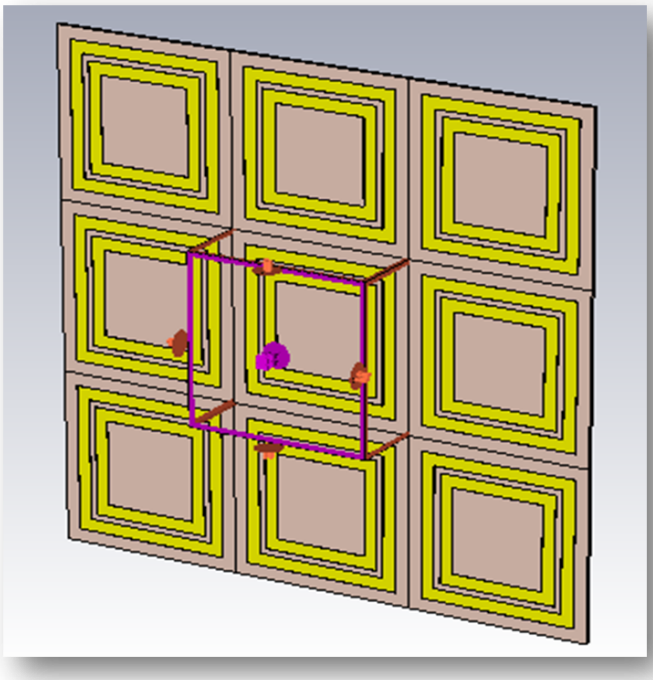

a) Periodic FSS

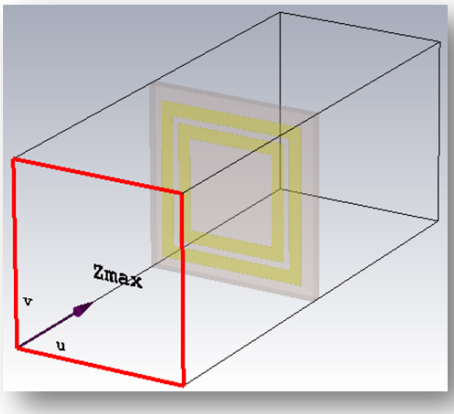

a) Unit cell

Figure 3.2: a) periodic FSS, b) FSS model with incident plane wave

In Figure 3.3, the transmission and reflection coefficients are presented for TM polarization for 0^0 and 45^0 angle of incidence. The resonant frequencies at 0^0 are 932.8 MHz and 1825.6 MHz, while at 45^0, these are 947.2 MHz and 1750 MHz, respectively. The corresponding transmission coefficients are -28 dB, -42 dB at 0^0, and -25 dB and -38 dB at 45^0. The shift in resonant frequency from 0^0 to 45^0 is about 14.4 MHz at band 900 MHz and about -75.6 MHz at band 1800 MHz . This shows that FSS has a stable frequency response as the angle of incidence varied from 0^0 to 45^0. It is demonstrated that the shift in resonant frequencies is occurred due to the mutual coupling between the FSS elements.

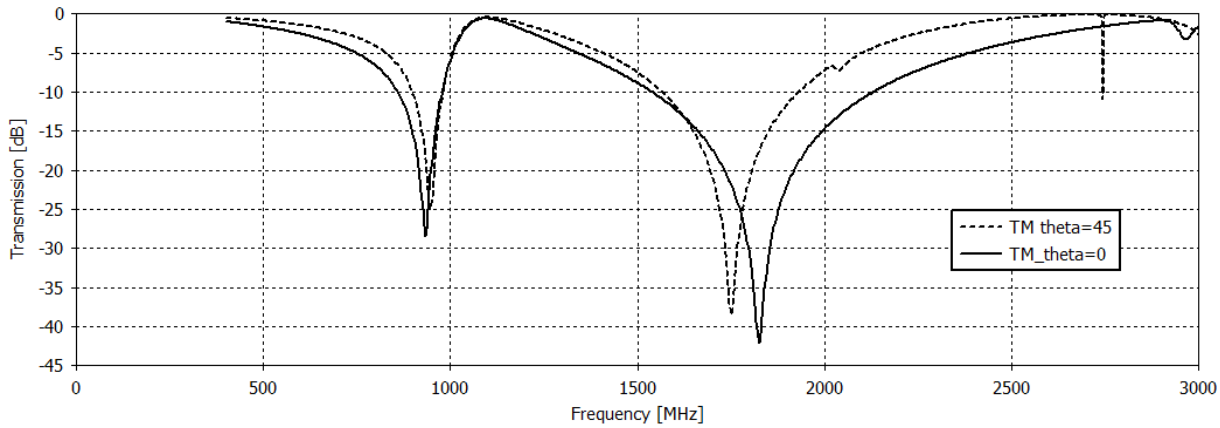

Figure 3.3: Simulation results of dual-bandstop FSS for TM polarization

In Figure 3.4, the transmission and reflection coefficients are presented for TE polarization for 0^0 and 45^0 angle of incidence. The resonant frequencies at 0^0 are 936.4 MHz and 1825.6 MHz, while at 45^0, these are 947.2 MHz and 1750 MHz, respectively. The corresponding transmission coefficients are -28 dB, -42 dB at0^0, and -25 dB and -38 dB at 45^0. The shift in resonant frequency from 0^0 to 45^0 is about 10.8 MHz at band 900 MHz and about -75.6 MHz at band 1800 MHz . This shows that FSS has a stable frequency response as the angle of incidence varied from 0^0 to 45^0. Tables 3.2 and 3.3 show simulation results for both TM and TE polarizations.

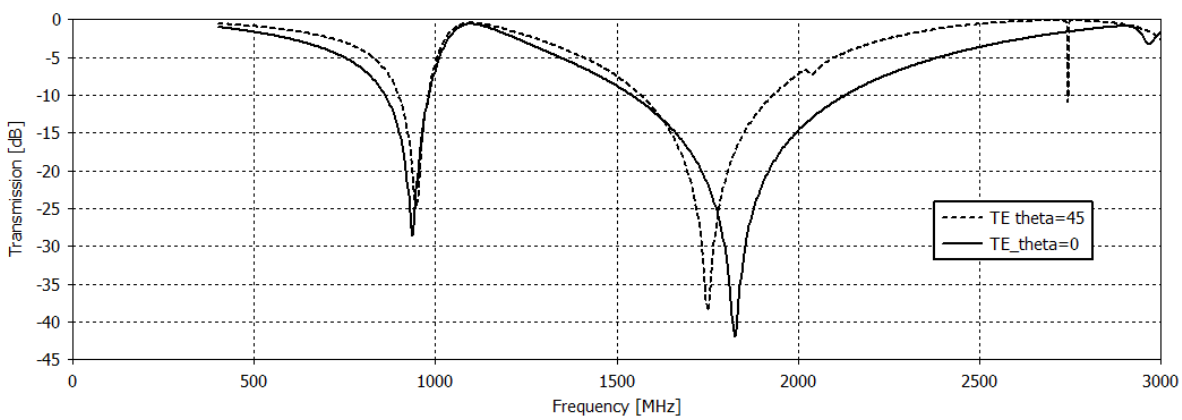

Figure 3.4: Simulation results of dual-bandstop FSS for TE polarization

Table 3.2: -10 dB transmission bandwidths at 900/1800 MHz for TM polarization

	900 MHz		1800 MHz	
Angle	Resonant frequency fr1 (MHz)	Bandwidth BW (MHz)	Resonant frequency fr2 (MHz)	Bandwidth BW (MHz)
TE 0^0	932.8	111	1825.6	588.6
TE 45^0	947.2	79	1750	457.7

Table 3.3: -10 dB transmission bandwidths at 900/1800 MHz for TE polarization

	900 MHz		1800 MHz	
Angle	Resonant frequency fr1 (MHz)	Bandwidth BW (MHz)	Resonant frequency fr2 (MHz)	Bandwidth BW (MHz)
TM 0^0	936.4	116.7	1825.6	574.2
TM 45^0	947.2	79.1	1750	357.7

3.5 Tri bandstop open loop FSS with FR substrate:

The second design for an FSS structure is presented in Figure 3.5. It is designed to cover three bands GSM900, GSM1800 and LTE.

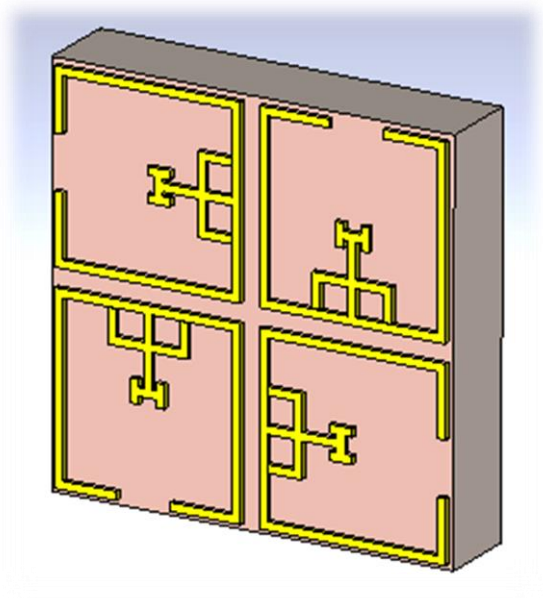

Figure 3.5: overall view of the unit cell model

3.5.1 Structure of FSS:

The unit cell dimensions of bandstop FSS are shown in Figure 3.6. The bandstop characteristics are achieved by designing several elements of different dimensions on FR-4 substrate. The periodicity of unit cell is $63.5\times63.5mm^2$. The circumference of the outer square open loop element is 103.9 mm which is tuned to 900 MHz while the remaining inner structure is tuned to 1800 MHz and LTE bands . The width of microstrip is 1.9 mm. Table 3.4 shows the dimensions of the structure in Figure 3.6.

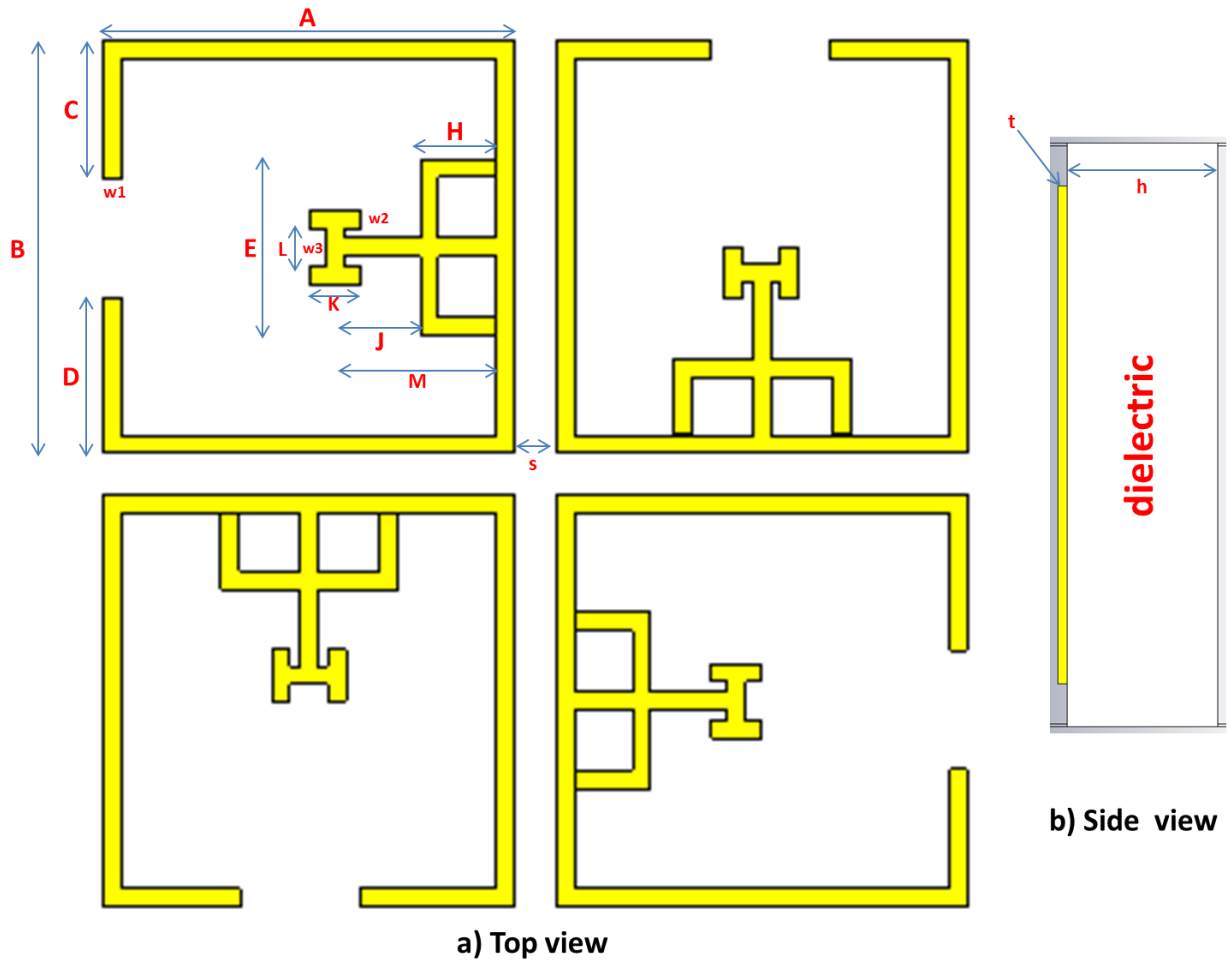

Figure 3.6: a) dimensions of top view model, b) side view of the model

Table 3.4: dimensions of the design

Name	A	B	C	D	E	H	J	h
Value (mm)	**29.4**	**29.4**	**9.8**	**11.08**	**12.59**	**5.41**	**5.46**	**1.6**
Name	w1	w2	w3	K	L	M	s	t
Value (mm)	**1.29**	**1.29**	**1.29**	**3.64**	**2.7**	**10.93**	**2.94**	**0. 1**

3.5.2 Simulation results:

The unit cell of FSS shown in Figure 3.7 is simulated by applying periodic boundary conditions using CST Microwave Studio. The transmission and reflection coefficients are obtained from 400-3000 MHz for both TE and TM polarizations at oblique incidences.

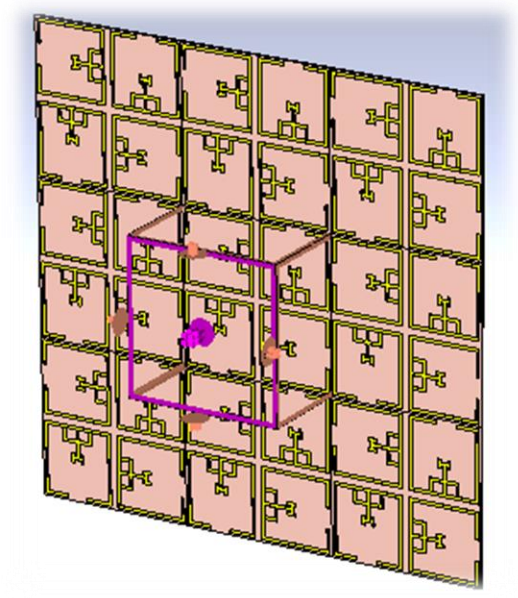

Figure 3.7: periodic cells

In Figure 3.8, the transmission and reflection coefficients are presented for TE polarization for 0^0 and 30^0 angle of incidence. The resonant frequencies at 0^0 are 939.4 MHz and 1813.6 MHz, 2740.5 MHz while at 30^0, these are 942.5 MHz and 1826 MHz, 2858.3 MHz . The corresponding transmission coefficients are -26 dB, -29 dB, -29 dB at 0^0, and -28 dB, -29 dB and -25 dB at 30^0. The shift in resonant frequency from 0^0 to 30^0 is about 3.1 MHz at 900 MHz, and 12.4 MHz at 1800 MHz This shows that FSS has a stable frequency response as the angle of incidence varied from 0^0 to 30^0 and also stable for more angles. But the shift at LTE band is about 117.8 MHz and increases at more angles as sown in Figure 3.8.

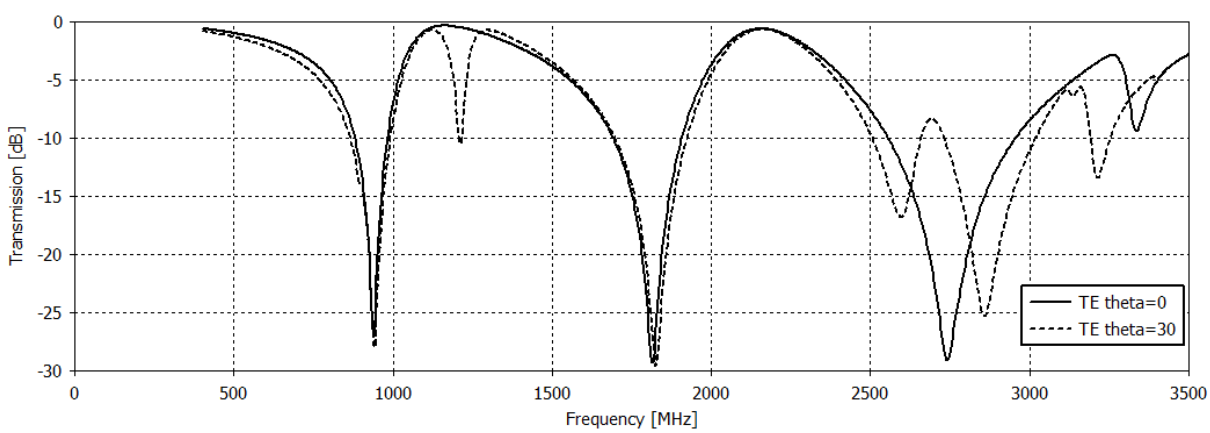

Figure 3.8: Simulation results of tri-bandstop FSS for TE polarization

In Figure 3.9, the transmission and reflection coefficients are presented for TM polarization for 0^0 and 30^0 angle of incidence. The resonant frequencies at 0^0 are 939.4 MHz, 1819.8 MHz and 2740.5 MHz, while at 30^0, these are 939.4 MHz, 1810.5 MHz and 2842.8 MHz, respectively. The corresponding transmission coefficients are -26 dB, -29 dB, -29 dB at 0^0, and -25 dB, -28 dB and -22 dB at 30^0. The shift in resonant frequency from 0^0 to 30^0 is about zero at 900 MHz. and -9.3 MHz at 1800 MHz This shows that FSS has a stable frequency response as the angle of incidence varied from 0^0 to 30^0. But the shift at LTE band is about 102.3 MHz and increases at more angles as sown in Figure 3.9. Therefore, it can be seen that the FSS response is sufficiently stable for both TE and TM polarizations as the angle of incidence is varied. Tables 3.5 and 3.6 and Figures 3.10, 3.11, 3.12 and 3.13 show simulation results for both TM and TE polarizations.

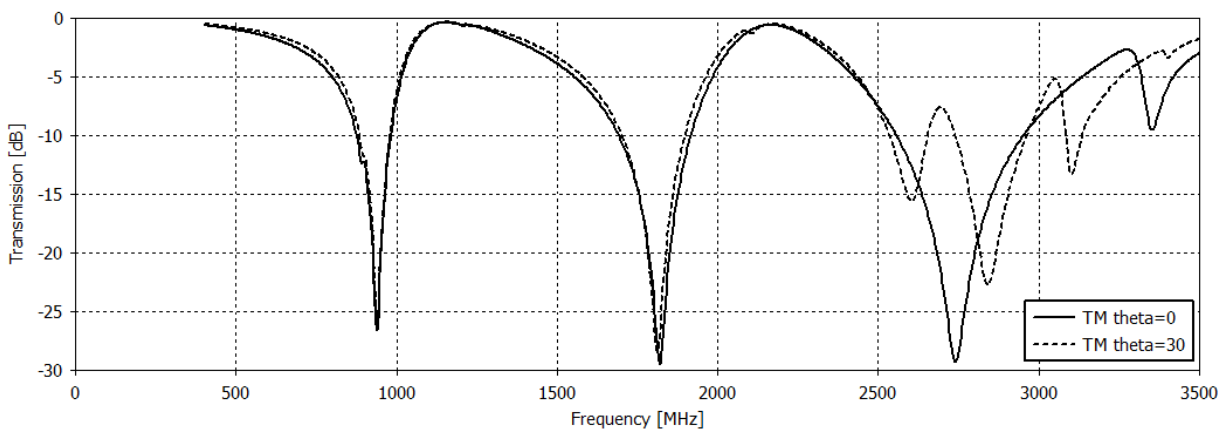

Figure 3.9: Simulation results of tri-bandstop FSS for TM polarization

Table 3.5: -10 dB transmission bandwidths at 900/1800 MHz and LTE Band for TE polarization

	900 MHz		1800 MHz		LTE Band	
Angle	Resonant frequency fr1 (MHz)	Bandwidth BW (MHz)	Resonant frequency fr2 (MHz)	Bandwidth BW (MHz)	Resonant frequency fr2 (MHz)	Bandwidth BW (MHz)
TE 0^0	939.4	98.8	1813.6	209.6	2740.5	390.2
TE 30^0	942.5	119.57	1826	220.6	2858.3	502.8

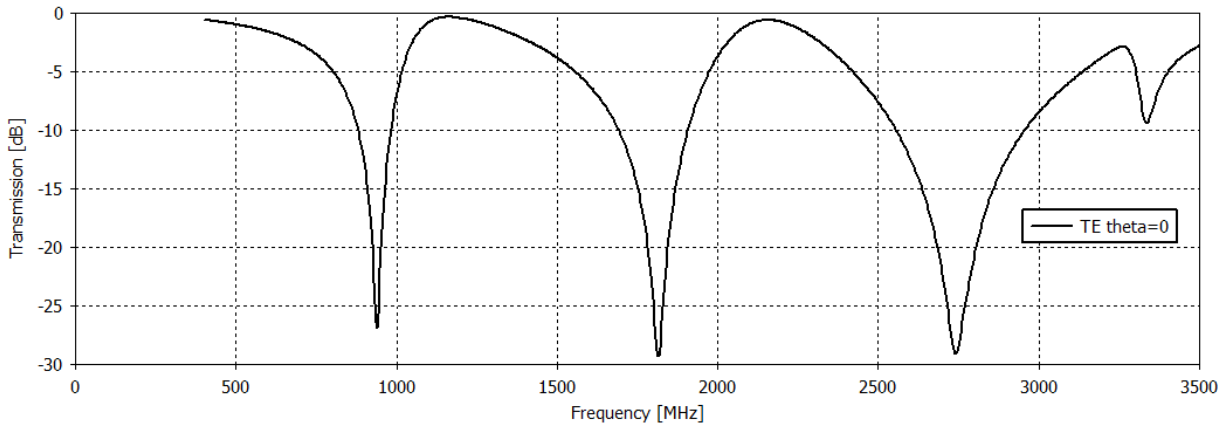

Figure 3.10: transmission bandwidths at 900/1800 MHz and LTE Band for TE polarization at theta=0

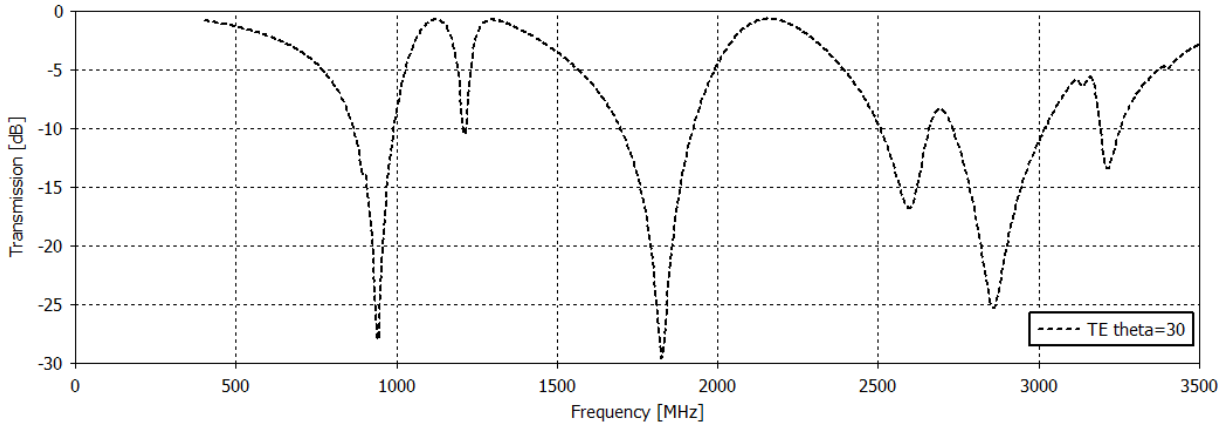

Figure 3.11: transmission bandwidths at 900/1800 MHz and LTE Band for TE polarization at theta=30

Table 3.6: : -10 dB transmission bandwidths at 900/1800 MHz and LTE Band for TM polarization

	900 MHz		1800 MHz		LTE Band	
Angle	Resonant frequency fr1 (MHz)	Bandwidth BW (MHz)	Resonant frequency fr2 (MHz)	Bandwidth BW (MHz)	Resonant frequency fr3 (MHz)	Bandwidth BW (MHz)
TM 0^0	939.4	104.2	1819.8	213.6	2740.5	382.7
TM 30^0	939.4	91.2	1810.5	186.3	2839.7	416.3

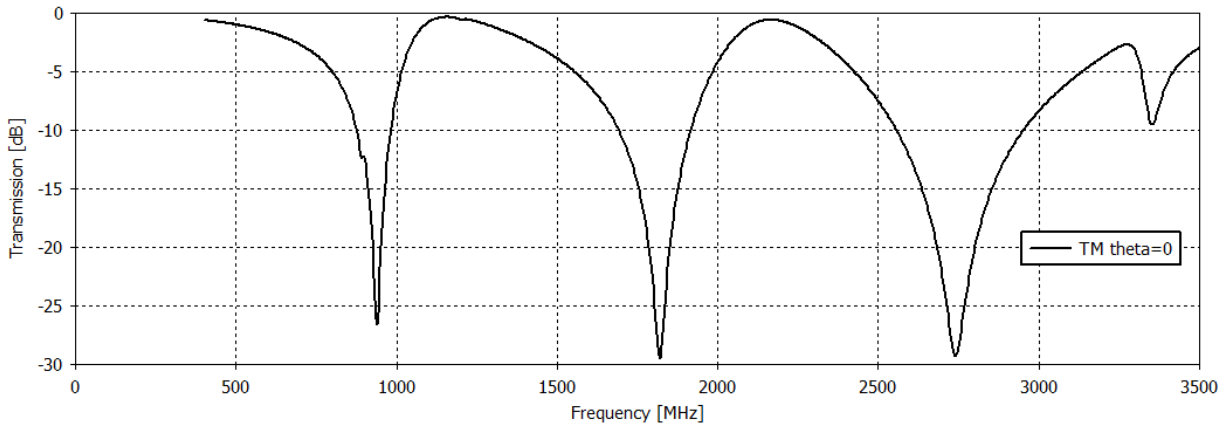

Figure 3.12: transmission bandwidths at 900/1800 MHz and LTE Band for TM polarization at theta=0

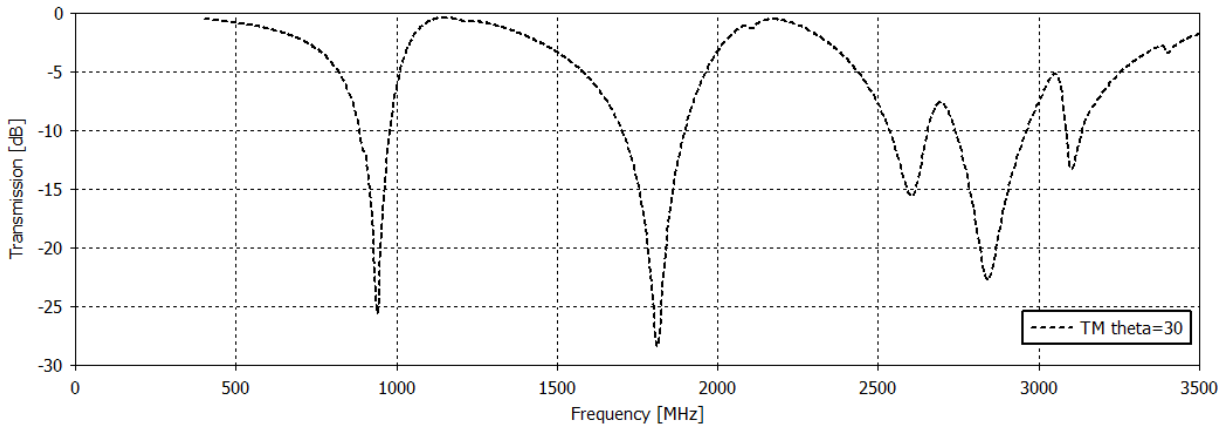

Figure 3.13: transmission bandwidths at 900/1800 MHz and LTE Band for TM polarization at theta=30

3.6 Tri bandstop open loop FSS with glass (pyrex) substrate:

Most of buildings have walls of glass that allows the unwanted signals to pass through it. This requires to design models on glass substrate to give the best results isolation. Figure 3.14 shows the third design for an FSS structure which etched in glass (pyrex) substrate and it is designed to cover three bands GSM900, GSM1800 and LTE.

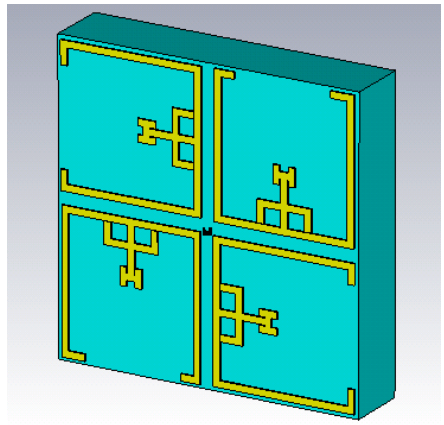

Figure 3.14: overall view of the unit cell model

3.6.1 Structure of FSS:

The unit cell dimensions of bandstop FSS are shown in Figure 3.14. The bandstop characteristics are achieved by designing several elements of different dimensions on Glass (Pyrex) substrate. The thickness of Pyrex substrate is 4 mm and the relative permittivity (ε_r) and a loss tangent (tan δ) are 4.82 and 0.0054, respectively. The periodicity of unit cell is 63.52×63.52 mm^2 . The width of all elements is 1.41 mm. The dimensions of the FSS structure are depicted in table 3.7.

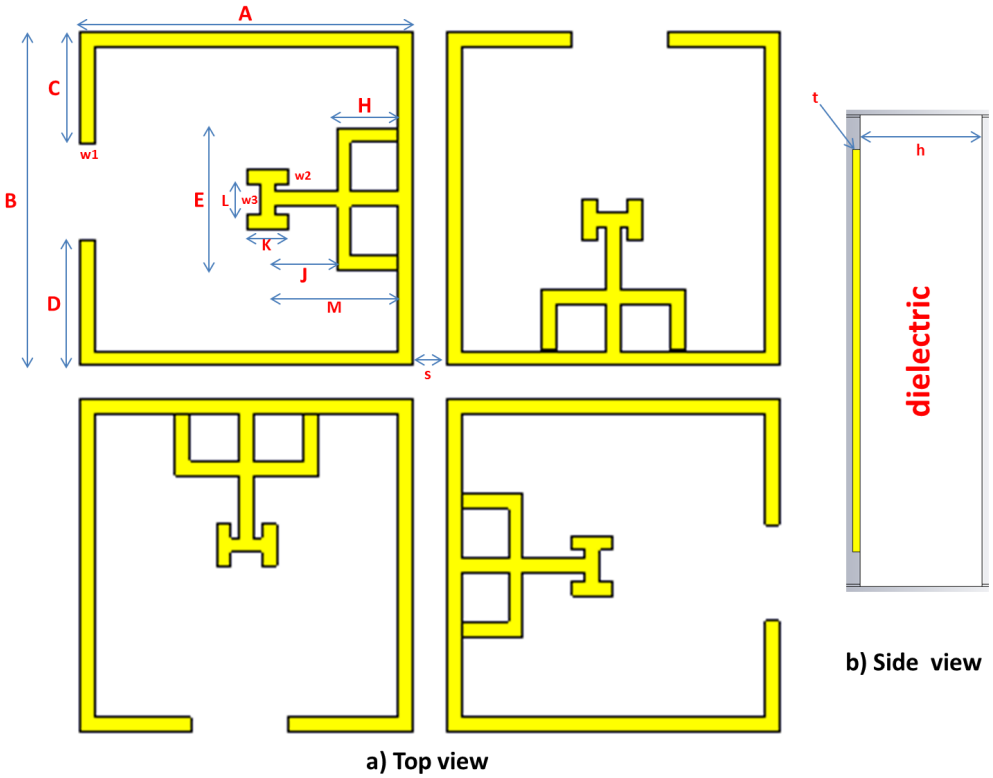

Figure 3.15: a) dimensions of top view model, b) side view of the model

Table 3.7: dimensions of the design

Name	A	B	C	D	E	H	J	h
Value (mm)	**29.4**	**29.4**	**4.9**	**4.22**	**11.36**	**4.64**	**4.7**	**4**
Name	w1	w2	w3	K	L	M	s	t
Value (mm)	**1.41**	**1.41**	**1.41**	**3.77**	**1.76**	**9.41**	**2.76**	**0.1**

3.6.2 Simulation results:

The transmission and reflection coefficients are obtained from 400-3500 MHz for both TE and TM polarizations at oblique incidences.

In Figure 3.16, the transmission and reflection coefficients are presented for TE polarization for 0^0 and 30^0 angle of incidence. The resonant frequencies at 0^0 are 958 MHz and 1832.2 MHz, 2712.6 MHz while at 30^0, these are 958 MHz and 1813.6 MHz, 2777.7 MHz. The corresponding transmission coefficients are -38.4 dB, -35.2 dB, -37.2 dB at 0^0, and -38 dB, -34.7 dB and -28.7 dB at30^0. The shift in resonant frequency from 0^0 to 30^0 is about zero MHz at 900 MHz . and -18.6 MHz at 1800 MHz This shows that FSS has a stable frequency response as the angle of incidence varied from 0^0 to 30^0 and also stable for more angles. But the shift at LTE band is about 65.1 MHz and increases at more angles as sown in Figure 3.16.

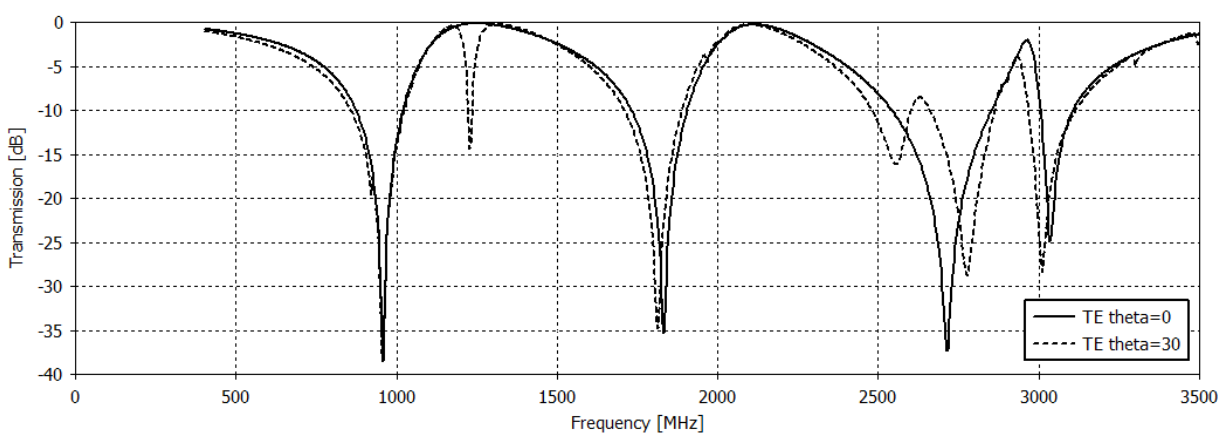

Figure 3.16: Simulation results of tri-bandstop FSS for TE polarization

In Figure 3.17, the transmission and reflection coefficients are presented for TM polarization for 0^0 and 30^0 angle of incidence. The resonant frequencies at 0^0 are 961.1 MHz, 1826 MHz and 2712.6 MHz, while at 30^0, these are 961.1 MHz, 1804.3 MHz and 2811.8 MHz, respectively. The corresponding transmission coefficients are -38.7 dB, -34.8 dB and -37 dB at 0^0, and -36.9

dB, -32.9 dB and -27.6 dB at 30^0. The shift in resonant frequency from 0^0 to 30^0 is about zero at 900 MHz, and -21.7 MHz at 1800 MHz . This shows that FSS has a stable frequency response as the angle of incidence varied from 0^0 to 30^0 and also stable for more angles. But the shift at LTE band is about 99.2 MHz and increases at more angles as shown in Figure 3.17. Therefore, it can be seen that the FSS response is sufficiently stable for both TE and TM polarizations as the angle of incidence is varied. Tables 3.8 and 3.9 and Figures 3.18, 3.19, 3.20 and 3.21 show simulation results for both TM and TE polarizations.

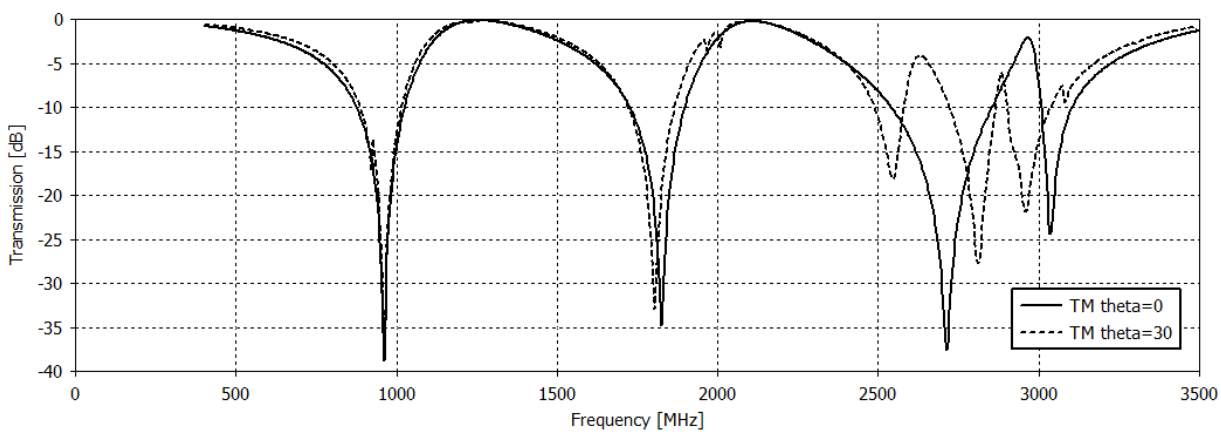

Figure 3.17: Simulation results of tri-bandstop FSS for TM polarization

Table 3.8: -10 dB transmission bandwidths at 900/1800 MHz and LTE Band for TE polarization

	900 MHz		1800 MHz		LTE Band	
Angle	Resonant frequency fr1 (MHz)	Bandwidth BW (MHz)	Resonant frequency fr2 (MHz)	Bandwidth BW (MHz)	Resonant frequency fr2 (MHz)	Bandwidth BW (MHz)
TE 0^0	958	139.84	1832.2	167.8	2712.6	301.4
TE 30^0	958	162.09	1813.6	173.3	2777.7	undefined

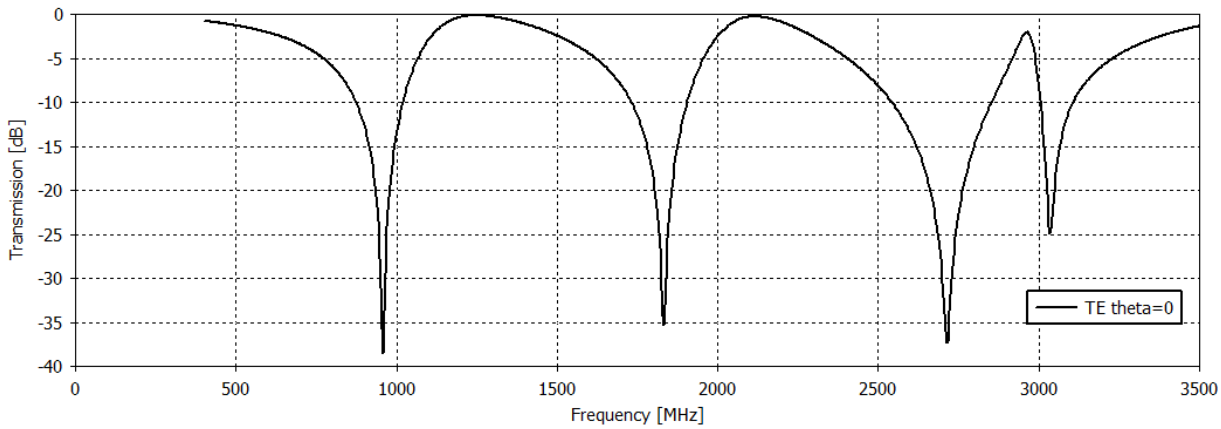

Figure 3.18: transmission bandwidths at 900/1800 MHz and LTE Band for TE polarization at theta=0

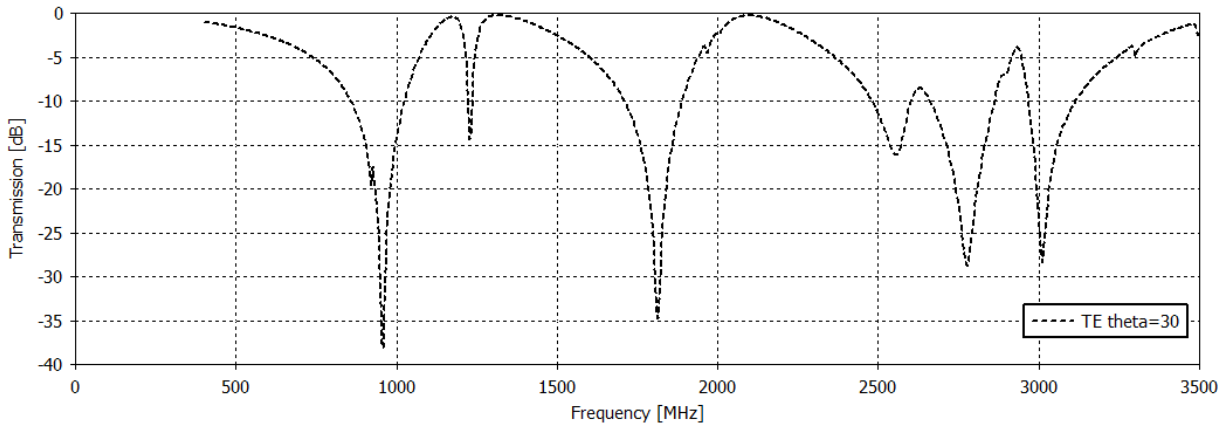

Figure 3.19: transmission bandwidths at 900/1800 MHz and LTE Band for TE polarization at theta=30

Table 3.9 : -10 dB transmission bandwidths at 900/1800 MHz and LTE Band for TM polarization

	900 MHz		1800 MHz		LTE Band	
Angle	Resonant frequency fr1 (MHz)	Bandwidth BW (MHz)	Resonant frequency fr2 (MHz)	Bandwidth BW (MHz)	Resonant frequency fr3 (MHz)	Bandwidth BW (MHz)
TM 0^0	961.1	143.1	1826	169.1	2712.6	310
TM 30^0	961.1	123.4	1804.3	138.2	2811.8	undefined

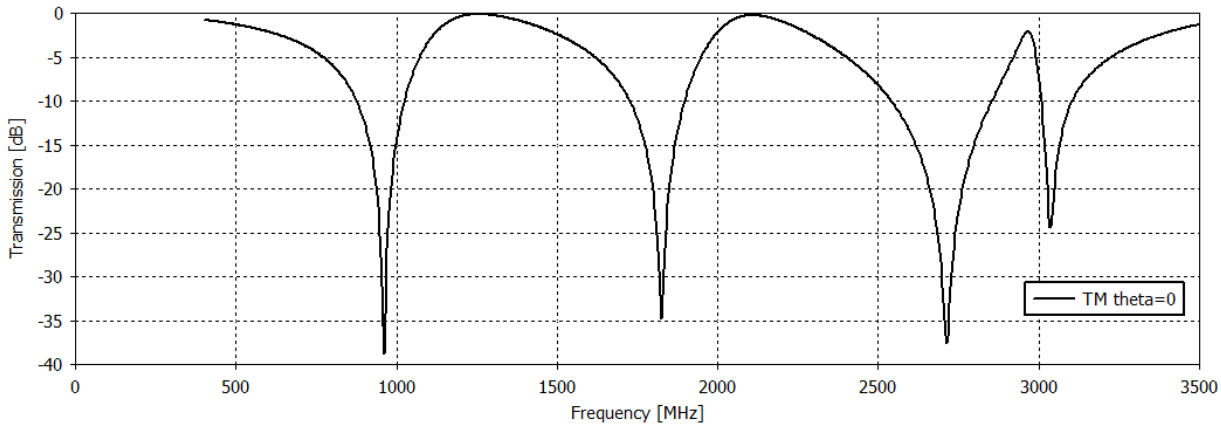

Figure 3.20: transmission bandwidths at 900/1800 MHz and LTE Band for TM polarization at theta=0

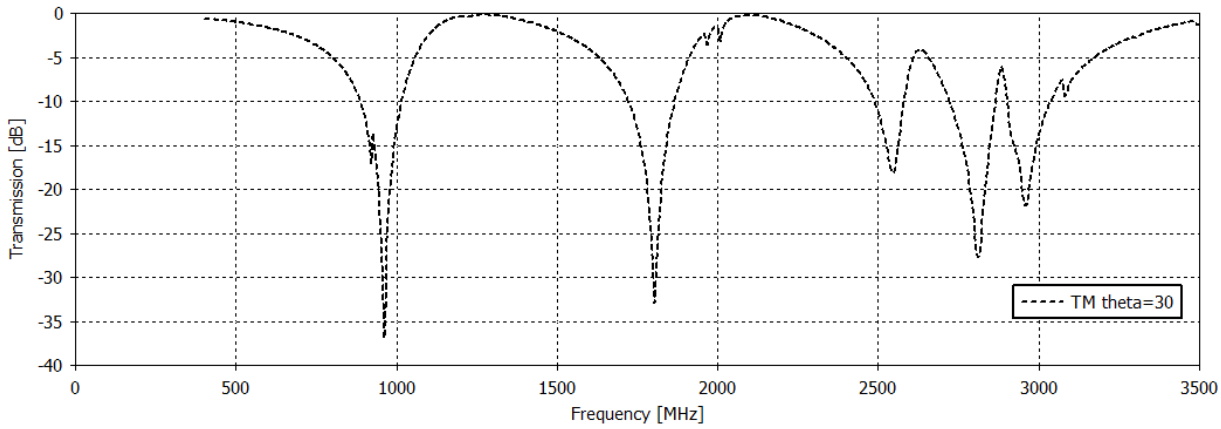

Figure 3.21: transmission bandwidths at 900/1800 MHz and LTE Band for TM polarization at theta=30

3.7 Quad bandstop E_shape FSS:

The fourth design for an FSS structure is presented in Figure 3.22. It is designed to cover four bands GSM900, GSM1800, 3G and LTE at normal incidence.

3.7.1 Structure of FSS:

The unit cell dimensions of bandstop FSS are shown in Figure 3.22. The bandstop characteristics are achieved by designing several elements of different dimensions on FR-4

substrate. The thickness of FR-4 substrate is 3.2 mm and the relative permittivity (ε_r) and the loss tangent (tan δ) are 4.3 and 0.02, respectively. The periodicity of unit cell is 63.5×63.5 mm^2 . The circumference of the outer square open loop element is 103.9 mm which is tuned to 900 MHz while the other dimensions of the structure are tuned to 1800 MHz, 3G and LTE band . The width of all microstrip elements is 1.9 mm. The dimensions of the FSS structure are depicted in table 3.10.

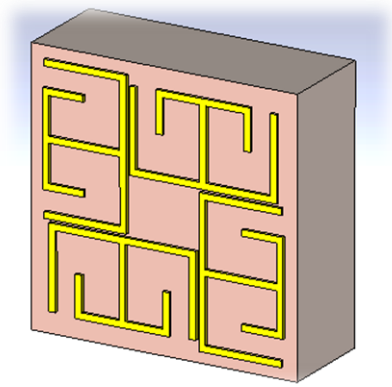

Figure 3.22: overall view of the unit cell model

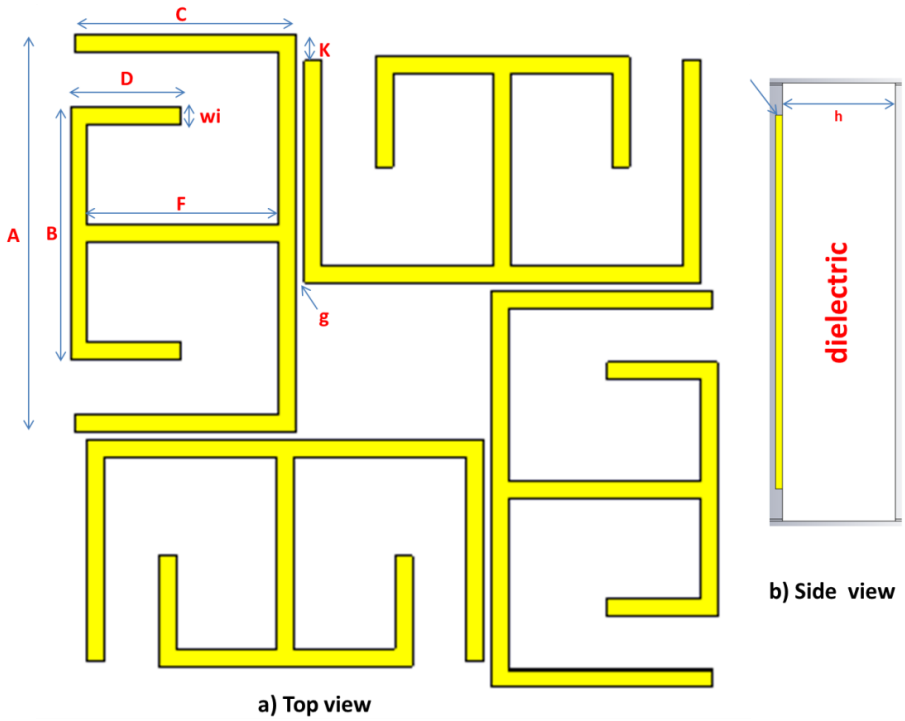

Figure 3.23: a) dimensions of top view model, b) side view of the model

Table 3.10: dimensions of the design

Name	A	B	C	D	F
Value (mm)	**55.31**	**35.42**	**30.95**	**15.43**	**26.76**
Name	K	w	g	h	t
Value (mm)	**3.56**	**2.4**	**1.15**	**3.2**	**0. 1**

3.7.2 Simulation results:

The unit cell of FSS is shown in Figure 3.24. The transmission and reflection coefficients are obtained from 400-3000 MHz for both TE and TM polarizations at normal incidence.

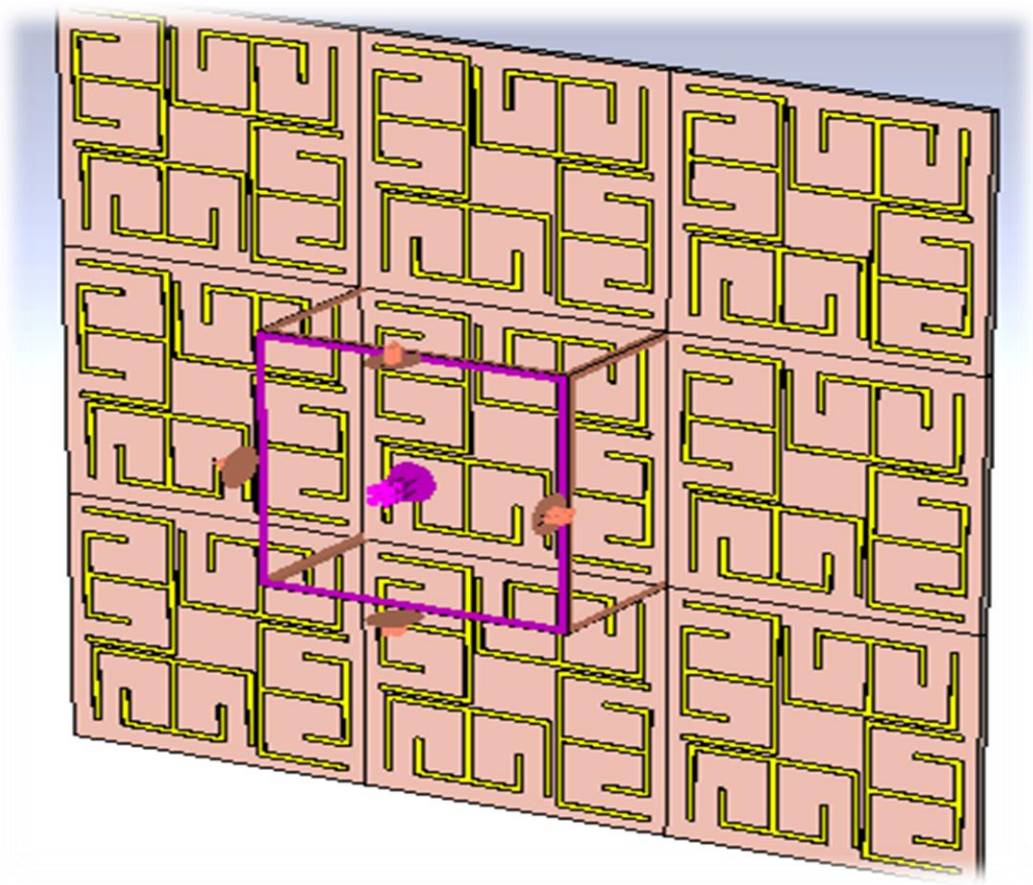

Figure 3.24: periodic cells

In Figure 3.25, the transmission and reflection coefficients are presented for TE polarization normal incidence. The resonant frequencies are 922.6 MHz (for GSM900), 2048.4 MHz (for

GSM1800 and 3G) and 2591.8 MHz (for LTE). The corresponding transmission coefficients are -24.5 dB, -34.2 dB, -25.2 dB respectively.

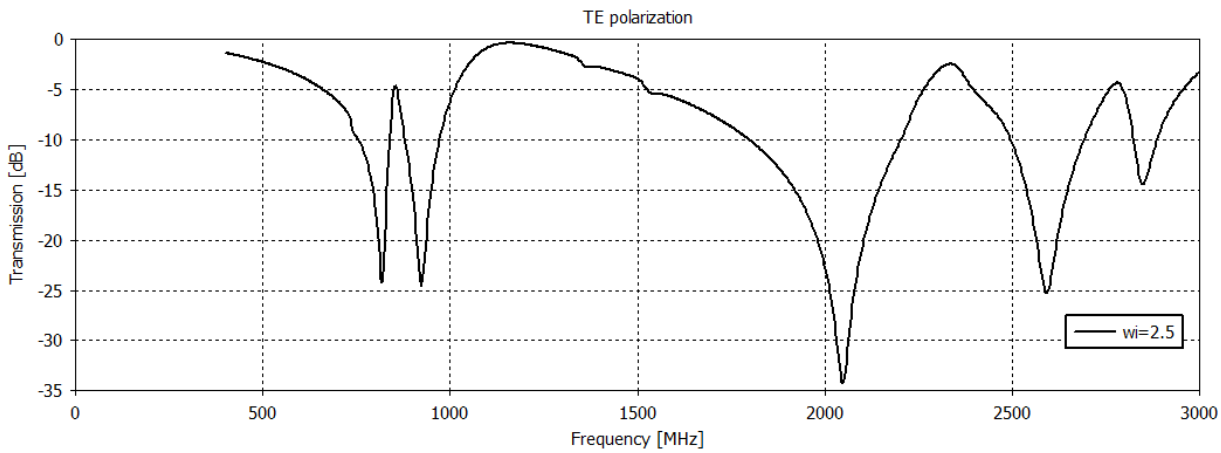

Figure 3.25: Simulation results of quad-bandstop FSS for TE polarization

3.7.3 The effect of changing the widths of elements:

As shown in Figure 3.26, the bandwidth and resonant frequency of the first band (900MHz) is still stable with varying the elements width from 2mm to 2.5mm. But this variation enhance the bandwidth of 1800MHz/3G band from 355 MHz at wi= 2 mm to 403 MHz at wi=2.5 mm. In the last band (LTE) the bandwidth is almost fixed, but the resonant frequency increases from 2563.2 MHz at wi=2 mm to 2591.8 MHz at wi=2.5 mm.

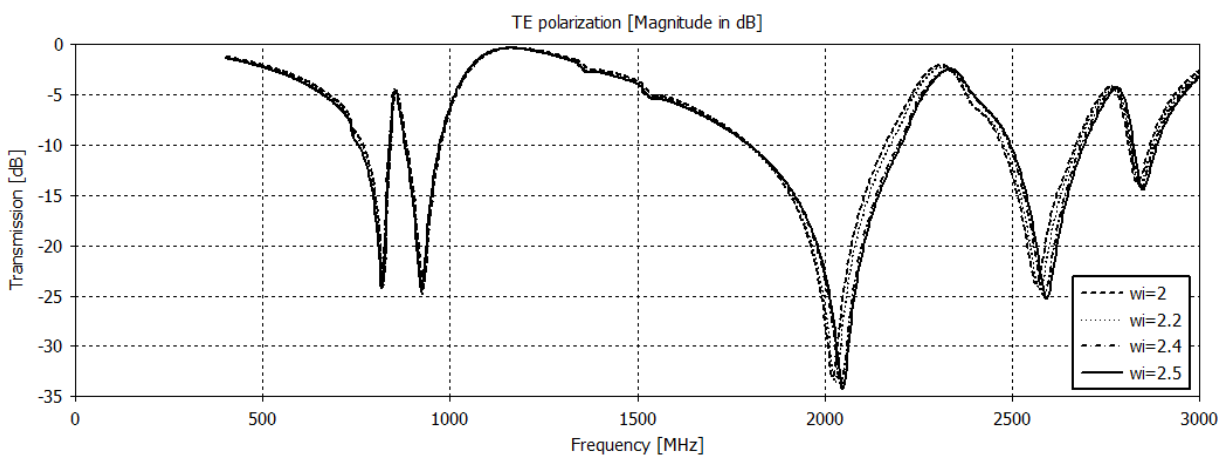

Figure 3.26: Simulation results of quad-bandstop FSS for TE polarization with varying the elements width

From comparison of TE polarization with TM polarization shown in Figure 3.27, we notice the shifting in resonant frequency in 900 MHz band with 8 MHz, but the shift is bigger in

1800 MHz/3G band which is about 109 MHz which leads to be the TM polarization is not stable for the all desired band.

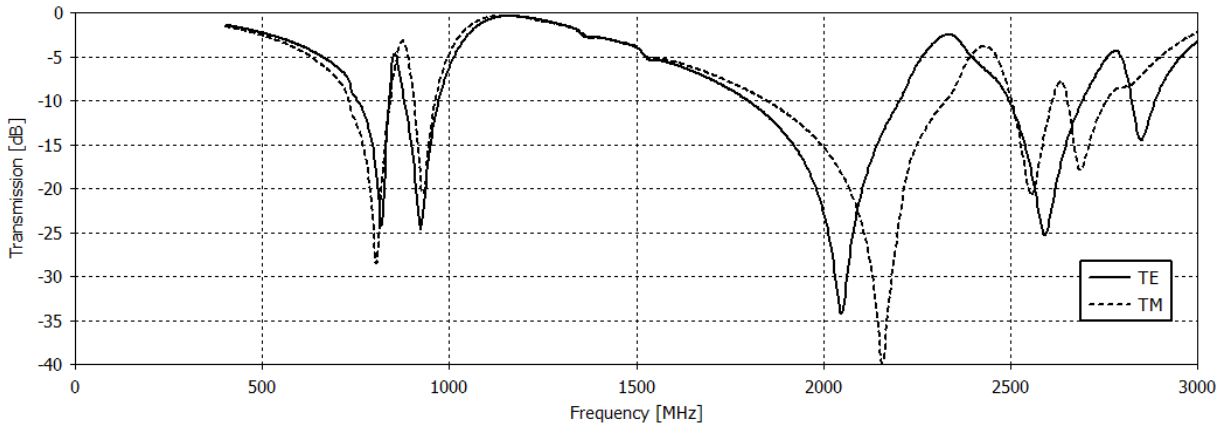

Figure 3.27: comparison between TE and TM polarization

3.8 Dual Bandstop double wired square loop FSS:

The new structure which is shown in the Figure 3.28 is a set of double square copper cells interconnected by iron cylinders, copper is used to obtain the desired frequency and to cover the bands 900/1800 and 3G. The copper elements are a cylindrical wire with diameter r2 formed as a square cells with soft angles which is shown with yellow color in Figure 3.28

The iron metal was used in the design to connect the copper square cells with each other without affecting the desired resonant frequency because it is a lossy metal. The iron elements are a cylindrical shape with diameter r1. The surrounding environment of FSS is air with ε_r is 1.00059. The feature of this design is ease of formation and can be built and used in open areas. The dimensions of the FSS structure are depicted in table 3.11.

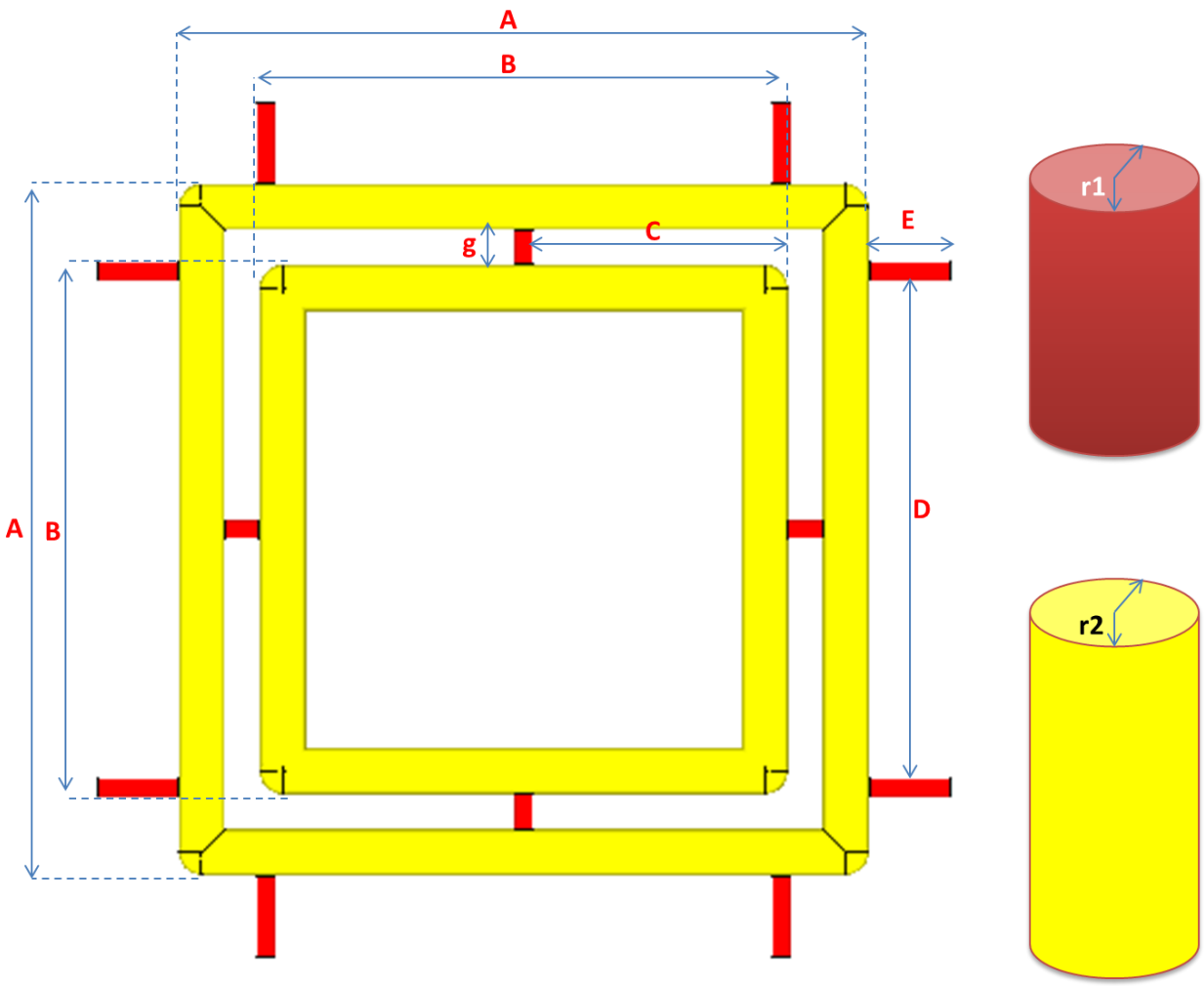

Figure 3.28: dimensions of top view model

Table 3.11: dimensions of the design

Name	A	B	C	D	E	g	r1	r2
Value (mm)	**75.21**	**54.6**	**26.31**	**54.17**	**8.7**	**5.19**	**1**	**2.5**

3.8.1 Structure of FSS:

The unit cell structure of bandstop FSS is shown in Figure 3.29. The bandstop characteristics are achieved by designing several elements of different dimensions. The periodicity of unit cell is 92.7×92.7 mm^2 . The outer square loop is tuned to 900 MHz while the inner square loop is tuned to 1800 MHz and 3G band. The diameter of the wire used to form the elements is 5 mm. the iron metal elements are used in the design as support to join the square loops together in a fixed structure.

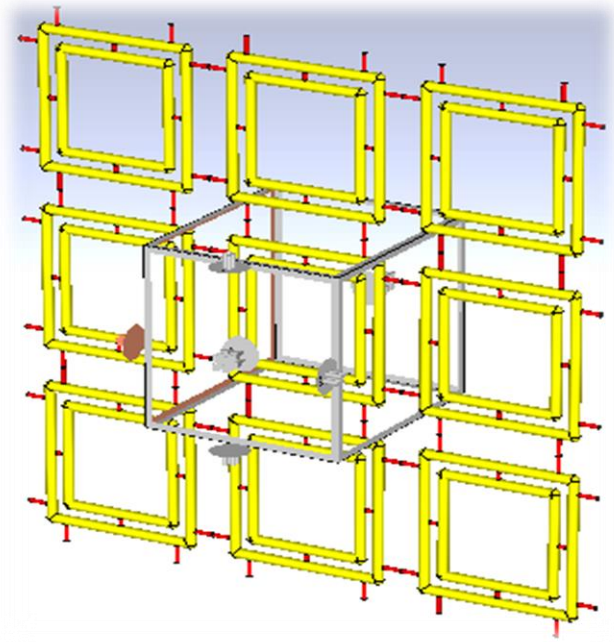

Figure 3.29: periodic square cells

3.8.2 Simulation results:

The transmission and reflection coefficients are obtained from 400 to 2600 MHz for both TE and TM polarizations.

In Figure 3.30, the transmission and reflection coefficients are presented for TE polarization for 0^0 and 30^0 angle of incidence. The resonant frequencies at 0^0 are 972.4 MHz and 1994.8 MHz, while at 30^0, these are 965.2 MHz and 1973.2 MHz respectively. The corresponding transmission coefficients are -55.4 dB, -58.1 dB at 0^0, and -54 dB, -59.7 dB at 30^0. The shift in resonant frequency from 0^0 to 30^0 is about -7.2 MHz at 900 MHz. and -21.6 MHz at 1800 MHz/3G This shows that FSS has a stable frequency response as the angle of incidence varied from 0^0 to 30^0.

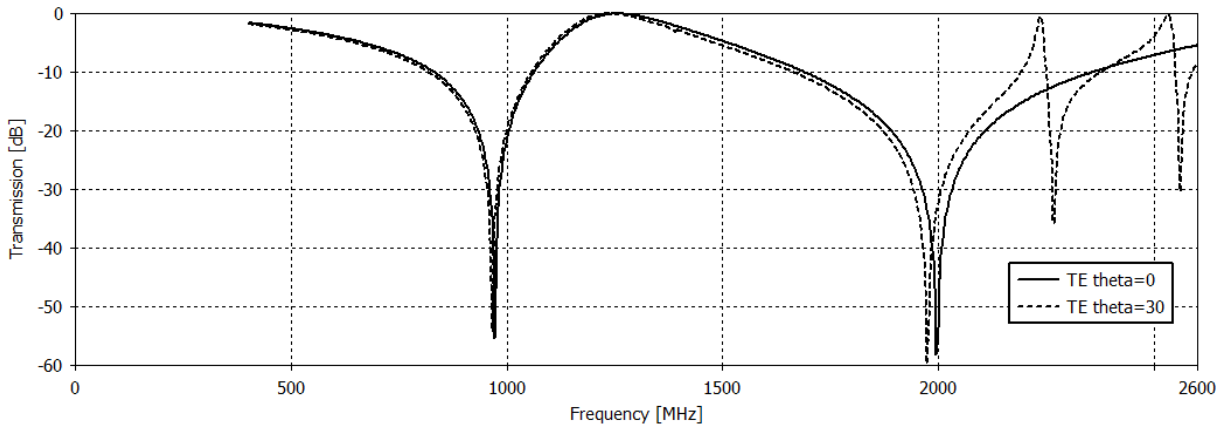

Figure 3.30: Simulation results of tri-bandstop FSS for TE polarization

In Figure 3.31, the transmission and reflection coefficients are presented for TM polarization for 0^0 and 30^0 angle of incidence. The resonant frequencies at 0^0 are 972.4 MHz, 1994.8 MHz, while at 30^0, these are 990.4 MHz, 1926.4 MHz. The corresponding transmission coefficients are -52.5 dB, -58.7 dB at 0^0, and -52.4 dB, -57.5 dB at 30, respectively. The shift in resonant frequency from 0^0 to 30^0 is about 18 MHz at 900 MHz, and -68.4 MHz at 1800 MHz/3G This shows that FSS has a stable frequency response as the angle of incidence varied from 0^0 to 30^0. Therefore, it can be seen that the FSS response is sufficiently stable for both TE and TM polarizations as the angle of incidence is varied.

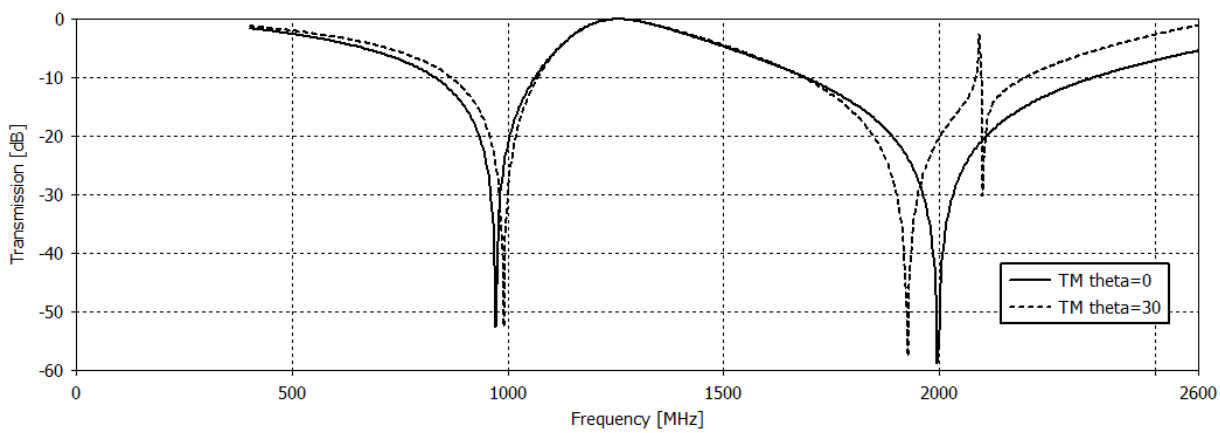

Figure 3.31: Simulation results of tri-bandstop FSS for TM polarization

Figures 3.32 and 3.33 show that the resonant frequencies are stable over TE and TM polarizations, but when the angle increases to 30^0 the resonant frequencies shifted by 25.2 MHz at band 900MHz, and shifted by -46.8 MHz at band 1800/3G. Tables 3.12 and 3.13 show simulation results for both TM and TE polarizations.

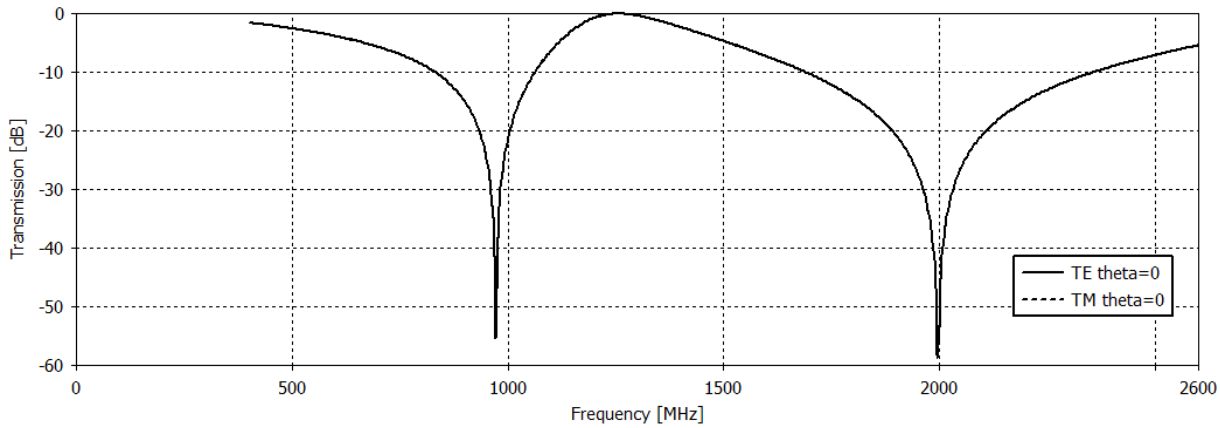

Figure 3.32: TE and TM polarization at theta=0

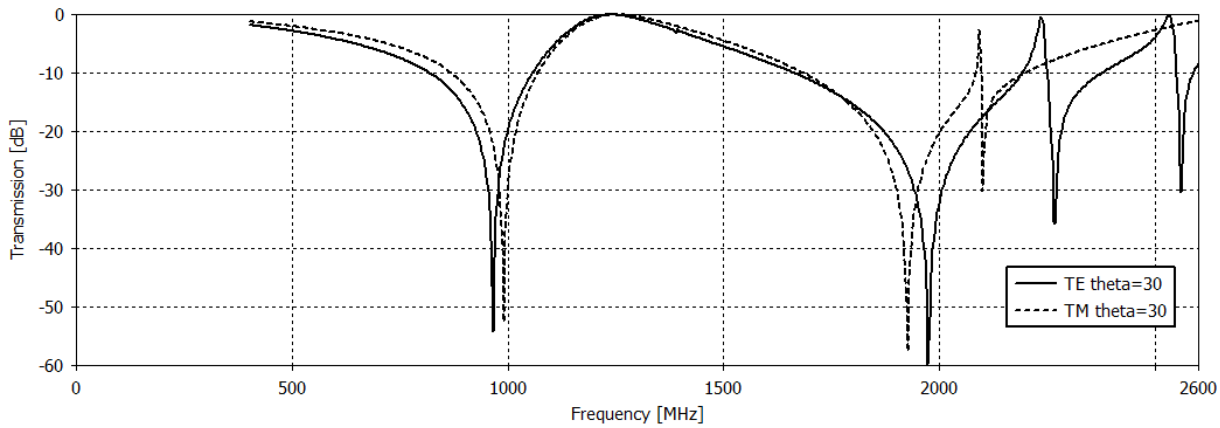

Figure 3.33: TE and TM polarization at theta=40

Table 3.12: -10 dB transmission bandwidths at 900/1800 MHz and 3G Band for TE polarization

	900 MHz		1800 MHz/3G	
Angle	Resonant frequency fr1 (MHz)	Bandwidth BW (MHz)	Resonant frequency fr2 (MHz)	Bandwidth BW (MHz)
TE 0^0	972.4	225.3	1994.8	639.8
TE 30^0	965.2	226.4	1973.2	503

Table 3.13: -10 dB transmission bandwidths at 900/1800 MHz and LTE Band for TM polarization

	900 MHz		1800 MHz	
Angle	Resonant frequency fr1 (MHz)	Bandwidth BW (MHz)	Resonant frequency fr2 (MHz)	Bandwidth BW (MHz)
TM 0^0	972.4	221	1994.8	626
TM 30^0	990.4	186	1926.4	478

Chapter 4: Conclusion

4.1 Summary:

The main purpose of this project is the analysis and design of microstrip frequency selective surfaces and wire net structures to shield the GSM frequencies and transmit the other frequencies. The other purposes that added to include other mobile systems such as 3G and LTE. New five structures are designed. The FSSs are almost unchanged when the incident angle is increased from 0^0 to 30^0 for both TE and TM polarizations. Tables from 4.1 to 4.9 show the transmission coefficients at desired frequencies of the project.

4.1.1 First design (Bandstop double square loop FSS):

Table 4.1 and 4.2 show that the deference in s_{21} between TE and TM polarization little at desired frequency and the result is stable when the incident angle changes from zero to 45^0

Table 4.1: s_{21} (dB) at desired frequencies at theta = 0^0

	GSM 900		**GSM 1800**	
	925 MHz	960 MHz	1805 MHz	1880 MHz
TE 0^0	-23	-16	-32	-24
TM0^0	-24	-15	-32	-24

Table 4.2: Table 1:s_{21} (dB) at desired frequencies at theta = 45^0

	GSM 900		**GSM 1800**	
	925 MHz	960 MHz	1805 MHz	1880 MHz
TE 45^0	-22	-18	-20	-19
TM 45^0	-15	-17	-20	-12

4.1.2 Second design (Tri bandstop open loop FSS with FR substrate):

We show that the transmission coefficients is stable over the three required bands at theta = 0^0 as shown in table 4.3, but the required results not valid when theta changes to 30^0 at LTE band as shown in Table 4.4.

Table 4.3: s_{21} (dB) at desired frequencies at theta = 0^0

	GSM 900		**GSM 1800**		**LTE**	
	925 MHz	960 MHz	1805 MHz	1880 MHz	2620 MHz	2690 MHz
TE 0^0	-20.2	-16.2	-26.9	-13.2	-13.7	-20.7
TM 0^0	-19.8	-16	-25.3	-14	-13.7	-20.9

Table 4.4: s_{21} (dB) at desired frequencies at theta = 30^0

	GSM 900		GSM 1800		LTE	
	925 MHz	960 MHz	1805 MHz	1880 MHz	2620 MHz	2690 MHz
TE 30^0	-20.3	-18.5	-23.5	-15.4	-15	-8.3
TM 30^0	-18.5	-15.5	-27	-12	-14	-7.6

4.1.3 Third design (Tri bandstop open loop FSS with glass (pyrex) substrate)

It shown in Table 4.5 the stability and good results of the transmission coefficients at the three required bands when theta = 0^0, but when theta changes to 30^0 the LTE band became not stable and the required s_{21} at all GSM 1800 band not valid as shown in Table 4.6.

Table 4.5: s_{21} (dB) at desired frequencies at theta = 0^0

	GSM 900		GSM 1800		LTE	
	925 MHz	960 MHz	1805 MHz	1880 MHz	2620 MHz	2690 MHz
TE 0^0	-17.1	-35.3	-20.18	-13.9	-15	-26.3
TM 0^0	-16.5	-37.6	-22.5	-12.5	-15.1	-26.8

Table 4.6: s_{21} (dB) at desired frequencies at theta = 30^0

	GSM 900		GSM 1800		LTE	
	925 MHz	960 MHz	1805 MHz	1880 MHz	2620 MHz	2690 MHz
TE 30^0	-17.5	-34.8	-29.7	-11.2	-8.6	-12.4
TM 30^0	-13.8	-35.4	-32.3	-8	-4.2	-7.2

4.1.4 Fourth design (Quad bandstop E_shape FSS)

In this design it is illustrated as shown in Table 4.7 that the good results achieved over four mobile bands at TE polarization when theta = 0^0, the required s_{21} results at TM polarization not valid at frequencies 1805 MHz and 2620 MHz.

Table 4.7:s_{21} (dB) at desired frequencies at theta = 0^0

	GSM 900		GSM 1800		3G		LTE	
	925 MHz	960 MHz	1805 MHz	1880 MHz	2110 MHz	2170 MHz	2620 MHz	2690 MHz
TE 0^0	-24	-12.2	-10.2	-13	-19	-12.6	-20	-10.2
TM 0^0	-20	-10.3	-9	-11	-25	-35	-8.7	-17.7

4.1.5 Fifth design (Dual Bandstop double wired square loop FSS):

Table 4.8 shows that the required s_{21} results achieved at TE and TM polarization and the results stills stable when theta changes from 0^0 to 30^0.

Table 4.8: s_{21} (dB) at desired frequencies at theta = 0^0

	GSM 900		**GSM 1800**		**3G**	
	925 MHz	960 MHz	1805 MHz	1880 MHz	2110 MHz	2170 MHz
TE 0^0	-18.2	-29.6	-14.5	-19.1	-19.7	-16.1
TM 0^0	-18.2	-29.8	-14.5	-19.1	-19.7	-16.1

Table 4.9: s_{21} (dB) at desired frequencies at theta = 30^0

	GSM 900		**GSM 1800**		**3G**	
	925 MHz	960 MHz	1805 MHz	1880 MHz	2110 MHz	2170 MHz
TE 30^0	-19.5	-36.2	-15.6	-20.7	-16.5	-12
TM 30^0	-14.4	-20.5	-16.2	-24.6	-17.2	-11.1

4.2 Future work:

- The 2D FSSs designed in this thesis could be fabricated in order to compare the simulation results and the measurement results.
- Transform the conventional passive FSSs into active ones by using lumped components.
- Design and fabricate 3D FSSs.

References

[1] D. Hu, “Introduction,” in 3D Frequency Selective Surfaces, vol. 98, Sheffield , United Kingdom, 2012, pp. 1–2.

[2] A. Munir, V. Fusco and O. Malyuskin, 'Tunable Frequency Selective Surfaces Characterisation', 2008 38th European Microwave Conference, 2008.

[3] Haiyan Chen, Xinyu Hou and Longjiang Deng, 'Design of Frequency-Selective Surfaces Radome for a Planar Slotted Waveguide Antenna', Antennas Wirel. Propag. Lett., vol. 8, pp. 1231-1233, 2009.

[4] G. Kiani and V. Dyadyuk, 'Low loss FSS polarizer for 70 GHz applications', Proceedings of the 2012 IEEE International Symposium on Antennas and Propagation, 2012.

[5] K. R. Jha, G. Singh, and R. Jyoti, “ A simple synthesis technique of single square loop frequency selective surface” Progress In Electromagnetics Research B, vol. 45, pp. 165–185, 2012.

[6] R. Dickie, R. Cahill, V. Fusco, H. Gamble and N. Mitchell, 'THz Frequency Selective Surface Filters for Earth Observation Remote Sensing Instruments', IEEE Transactions on Terahertz Science and Technology, vol. 1, no. 2, pp. 450-461, 2011.

[7] R. Dickie, R. Cahill, H. Gamble, V. Fusco, B. Moyna, P. Huggard, N. Grant and C. Philpot, 'Micromachined 300 GHz high Q resonant slot frequency selective surface filter', IEE Proceedings - Microwaves, Antennas and Propagation, vol. 151, no. 1, p. 31, 2004.

[8] Wikipedia, "1G", 2015. [Online]. Available: https://en.wikipedia.org/wiki/1G. [Accessed: 26- Dec- 2015].

[9] Wikipedia, "History of mobile phones", 2015. [Online]. Available: https://en.wikipedia.org/wiki/History_of_mobile_phones. [Accessed: 26- Dec- 2015].

[10] Globalspec.com, "Chapter 2: First Generation Analog Cellular | IHS Engineering360", 2015. [Online]. Available: http://www.globalspec.com/reference/52290/203279/chapter-2-first-generation-analog-cellular. [Accessed: 26- Dec- 2015].

[11] L. Aravamudhan, S. Faccin, R. Mononen, B. Patil, Y. Saifullah, S. Sharma and S. Sreemanthula, 'Second-Generation Mobile Networks | Getting to Know Wireless Networks and Technology | InformIT', Informit.com, 2015. [Online]. Available: http://www.informit.com/articles/article.aspx?p=98132&seqNum=4. [Accessed: 19- Nov- 2015].

[12] Slideshare.net, "Introduction to 3 g mobile communications (juha korhonen)", 2015. [Online]. Available: http://www.slideshare.net/tbutomo/introduction-to-3-g-mobile-communications-juha-korhonen. [Accessed: 26- Dec- 2015].

[13] A. Singh, "GSM & CDMA", Slideshare.net, 2015. [Online]. Available: http://www.slideshare.net/abhijeetsinghims/gsm-cdma-52837157. [Accessed: 26- Dec- 2015].

[14] Wikipedia, '3G', 2015. [Online]. Available: https://en.wikipedia.org/wiki/3G. [Accessed: 28- Nov- 2015].

[15] Arcelect.com, '2G - 3G Cellular Wireless GSM, GPRS, EDGE, W-CDMA,Â UMTS,Â TDMA, CDMA, CDMA2000 1xRTT, CDMA2000 1xEV-DO, and CDMA2000 1xEV-DV', 2015. [Online]. Available: http://www.arcelect.com/2G-3G_Cellular_Wireless.htm. [Accessed: 20- Nov- 2015].

[16] T. Zacharopoulou, 'Why LTE is a success? LTE vs WiMAX', 0el70lte, 2012. [Online]. Available: https://0el70lte.wordpress.com/2012/06/29/why-lte-is-a-success-lte-vs-wimax/. [Accessed: 23- Nov- 2015].

[17] 4gamericas.org, '4gamericas :: Statistics - Global', 2015. [Online]. Available: http://www.4gamericas.org/en/resources/statistics/statistics-global/. [Accessed: 23- Nov- 2015].

[18] Molisch, Andreas (2010). Wireless communications(2. ed.). Oxford: Wiley- Blackwell. p. 591. ISBN 978-0-470-74186-3. Retrieved 29 January 2015

[19] Worldtimezone.com, 'GSM World Coverage Map- GSM Country List by frequency bands', 2015. [Online]. Available: http://www.worldtimezone.com/gsm.html. [Accessed: 27- Nov- 2015].

[20] Radio-electronics.com, 'UMTS Frequency Bands | 3G WCDMA UARFCN | Radio-Electronics.Com', 2015. [Online]. Available: http://www.radio-electronics.com/info/cellulartelecomms/umts/umts-wcdma-frequency-bands-frequencies.php. [Accessed: 28- Nov- 2015].

[21] Radio-electronics.com, 'LTE Bands | LTE Frequency Bands Spectrum | Radio-Electronics.com', 2015. [Online]. Available: http://www.radio-electronics.com/info/cellulartelecomms/lte-long-term-evolution/lte-frequency-spectrum.php. [Accessed: 28- Nov- 2015].

[22] Spectrummonitoring.com, 'List of Mobile Frequencies by Country (GSM, CDMA, UMTS, LTE)', 2015. [Online]. Available: http://www.spectrummonitoring.com/frequencies/. [Accessed: 28- Nov- 2015].

[23] Gsmarena.com, 'Network coverage in Israel - 2G/3G/4G mobile networks', 2015. [Online]. Available: http://www.gsmarena.com/network-bands.php3?sCountry=Israel. [Accessed: 28- Nov- 2015].

[24] F. Costa, A. Monorchio and G. Manara, "An Overview of Equivalent Circuit Modeling Techniques of Frequency Selective Surfaces and Metasurfaces", Applied Computational Electromagnetics Society Journal, vol. 29, no. 12, 2014.

[25] K. Sarabandi and N. Behdad, “A frequency selective surface with miniaturized elements,” IEEE Trans. Antennas Propag., vol. 55, pp. 1239-1245, May 2007.

[26] B. Hooberman, “Everything you ever wanted to know about frequency-selective surface filters but were afraid to ask,” May, 2005.

http://calvin.phys.columbia.edu/group_web/filter_development/download/filter.pdf and http://calvin.phys.columbia.edu/group_web/filter_development/download/References.pdf

[27] C. Lee and R. Langley, 'Equivalent-circuit models for frequency-selective surfaces at oblique angles of incidence', IEE Proc. H Microw. Antennas Propag. UK, vol. 132, no. 6, p. 395, 1985.

[28] MARCUVITZ , N. : 'Waveguide handbook ' (McGraw-Hill , 1951)

[29] R. Langley and E. Parker, 'Equivalent circuit model for arrays of square loops', Electron. Lett., vol. 18, no. 7, p. 294, 1982.

[30] Academia.edu, 'A New Equivalent Circuit Based FSS Design Method by Using Genetic Algorithm', 2015. [Online]. Available: https://www.academia.edu/723002/A_New_Equivalent_Circuit_Based_FSS_Design_Method_by_Using_Genetic_Algorithm. [Accessed: 11- Dec- 2015].

[31] W. Che, H. Ye, Y. Xiong, Y. Chang and C. Christopoulos, 'A fast and efficient method for design of circuit analog absorbers consisting of resistive square loop arrays', 2015 IEEE International Conference on Computational Electromagnetics, 2015.

[32] A. Campos and T. Silva, 'Spectral domain analysis of double screen frequency selective surfaces', Journal of Microwaves, Optoelectronics and Electromagnetic Applications, vol. 11, no. 1, pp. 81-92, 2012.

[33] A. Campos, R. Moreira and J. Trindade, "A comparison between the equivalent circuit model and moment method to analyze FSS", 2009 SBMO/IEEE MTT-S International Microwave and Optoelectronics Conference (IMOC), 2009.

[34] M. Hosseini and M. Hakkak, "Characteristics Estimation for Jerusalem Cross-Based Artificial Magnetic Conductors", Antennas Wirel. Propag. Lett., vol. 7, pp. 58-61, 2008.

[35] D. Singh, A. Kumar, S. Meena and V. Agrawala, " Analysis of frequency selective surfaces for radar absorbing materials ", Progress In Electromagnetics Research B, vol. 38, pp. 297-314, 2012.

[36] M. Aziz, M. Shukor, B. Ahmad, M. Suaidi, M. Johar, M. Othman, S. Salleh, F. Azmin and M. Malek, "Investigation of a square loop Frequency Selective Surface (FSS) on hybrid material at 2.4 GHz", 2013 IEEE International Conference on Control System, Computing and Engineering, 2013.

[37] M. Raspopoulos and S. Stavrou, "Frequency Selective Buildings Through Frequency Selective Surfaces", IEEE Trans. Antennas Propagat., vol. 59, no. 8, pp. 2998-3005, 2011.

[38] G. Sen, T. Mandal, S. Majumdar, S. Mahato, S. Mondal and P. Sarkar, "Design of a wide band Frequency Selective Surface (FSS) for multiband operation of reflector antenna", 2012 5th International Conference on Computers and Devices for Communication (CODEC), 2012.

[39] E. Yildirim and O. Civi, "Design of a wideband radar absorbing structure", Antennas and Propagation (EUCAP), Proceedings of the 5th European Conference on, pp. 1324-1327, 2011.

[40] T. Zhang, G. Yang, W. Li, Q. Jiang and Q. Wu, "Research on novel miniaturized frequency selective surfaces consist of rectangle spiral-based elements", 2010 Global Mobile Congress, 2010.

[41] Hui Lai Liu, K. Ford and R. Langley, "Design Methodology for a Miniaturized Frequency Selective Surface Using Lumped Reactive Components", IEEE Trans. Antennas Propagat., vol. 57, no. 9, pp. 2732-2738, 2009.

[42] Connection.ebscohost.com, "Selective Control of GSM 900 MHz, GSM 1800 MHz and ISM 2.4 GHz Communication inside Room using Tri-Band Jerusalem Cross Frequency Selective

Wall", 2015. [Online]. Available: http://connection.ebscohost.com/c/articles/99720180/selective-control-gsm-900-mhz-gsm-1800-mhz-ism-2-4-ghz-communication-inside-room-using-tri-band-jerusalem-cross-frequency-selective-wall. [Accessed: 18- Dec- 2015].

[43] E. Unal, A. Gokcen and Y. Kutlu, "Effective electromagnetic shielding", IEEE Microwave Magazine, vol. 7, no. 4, pp. 48-54, 2006.

[44] Cst.com, "CST - Computer Simulation Technology", 2016. [Online]. Available: https://www.cst.com/. [Accessed: 08- Jan- 2016].